Electrical Characterization of GaN:Si and AlGaN:Si

Hong Ye

Hongy@student.chalmers.se

Department of Applied Physics

Department of Microtechnology and Nanoscience

CHALMERS UNIVERSITY OF TECHNOLOGY

Göteborg, Sweden 2011

Abstract

Wide band gap materials such as GaN, AlN and AlGaN alloys are of great interest because of their special physical properties which are very suitable for optoelectronic and electronic device applications. The group-III-nitride semiconductors are the only semiconductor materials capable of emitting light from the infrared ($E_{g,InN} = 0.7\ eV$) to the deep ultraviolet ($E_{g,AlN} = 6.2\ eV$) part of the spectrum. Compared to other semiconductors, III-nitrides also possess several other advantageous characteristics that are interesting for devices, such as high thermal conductivity, high breakdown voltage, and resistance to both high temperatures and chemically hostile environments.

This work is focused on Hall Effect measurements on GaN and AlGaN layers doped with Si. Bohr's hydrogen model is used as the basis for a discussion on the theory of the doping mechanism and its effects on the conductivity. The Hall Effect and the basic work principle of the Hall Effect setup are described. Hall Effect measurements are frequently employed in my diploma work to measure the resistivity, mobility and carrier concentration of our III-nitride samples. Molecular beam epitaxy (MBE) is used to grow GaN and AlGaN layers doped with Si. A solid source Si-cell that is mounted on the MBE system is used to provide the Si dopant. The atomic Si flux corresponding to the doping concentration is depending exponentially on the Si-cell temperature. The atomic Si flux (and consequentially also the electron concentration) in the MBE system is depending exponentially with the temperature. Temperature dependent Hall Effect measurements on a reference GaAs:Si sample are also performed as a comparison. It is demonstrated that (compared to GaAs) achieving a high carrier concentration in GaN and especially AlGaN is challenging since these materials have large bandgaps (>3.4 eV for AlGaN vs. 1.4 eV for GaAs). The large bandgap tends to increase the activation energy of the donor.

Keywords: III-V semiconductors, III-nitrides, GaN, AlGaN, Schottky contact, Ohmic contact, Si-doping, Bohr's hydrogen atom model, Hall Effect, Molecular beam epitaxy.

Acknowledgements

First and foremost, I would like to express my sincere gratitude to my supervisor, Professor Tommy Ive, for guiding me in the field of wide band gap semiconductors. Without his support and encouragement, this thesis would not have been possible.

Many thanks to all current and former members of the Microwave Electronics Laboratory for their help and friendship over the half years: Professor Thorvald Andersson for introducing me to the theory of semiconductor conductive properties; Dr Fredrik Fälth for taking those difficult first steps in Hall Effect measurements; Licentiate student Rashid Farivar for his scientific and technical assistance and fruitful discussions; last but definitely not the least, Lars-Åke Sidenberg for his helpful suggestion with the Hall Effect setup.

I am indebted to the PhD student David Adolph for his support and friendship. Sincere thanks to him for giving me advice on the way of thinking about not just the physic problem but also the essence of life. I wish to thank to Siham Doubaji for her cooperation and discussion on Capacitance-voltage measurement and really great friendship. I am grateful to everyone working in the Laboratory for providing a pleasant study and research environment.

Finally, sincere thanks to my parents and the whole families for all the support and care they have shown me. I would also like to extend my thanks to friends all over the world. In particular, my “family” here in Göteborg, Xiaoning Gong deserves special thanks for being the best of the friends. Warmest wishes to Hongming Cai families who have made my stay in Sweden a pleasurable experience.

Hong Ye

Sep. 2011

Contents

1. Introduction

1.1 History of semiconductors

According to G.Busch [1] the term “semiconducting” was first used by Alessandro Volta in 1782. The first documented observation of a semiconducting effect took place in 1833, when Michael Faraday described the decreased resistance of silver sulfide with temperature [2]. In 1874 Karl Ferdinand Braun detected rectification in metal sulfides using a metal point probe [3]. Later that year, Arthur Schuster found rectification in a storage circuit made of copper wires due to copper oxide at the ends of the wires. A new semiconductor copper oxide was discovered [4]. Among all the research on rectification later in that period, Walter Schottky’s research was outstanding for the experimental verification the presence of a barrier in a metal-semiconductor junction in 1929 [4].

Meanwhile, another physical property of semiconductors, namely the sensitivity to light attracted many physicists. In 1839, Alexander Edmund Becquerel discovered the photovoltaic effect at a junction between a semiconductor and an electrolyte [5]. While the photovoltaic effect in solids was observed almost forty years later by Adams and Day in 1876. They noticed that presence of light could change the direction of the current flowing through selenium connected to a battery [6]. With combination of a metal plate and a thin layer of selenium covered by a very thin layer of gold, the first working solar cell was constructed by Charles Fritts in 1883 [6].

Since Edwin Herbert Hall discovered the deflection of charge carriers in magnetic field in 1878, this phenomenon played an important role for further study of semiconductor properties [7]. From then on, a number of theories were developed: electrons in lattices developed by Ferdinand Bloch in 1928; the concept of forbidden gaps by Rudolf Peierls in 1930; conduction caused by impurities by Alan Wilson in 1931; the concept of hole by Heisenberg in 1931 and thermionic emission by Hans Bethe in 1942 [7].

The III-V nitrides are not really novel materials. Early in 1907, the synthesis of AlN was already reported and it is believed to be one of the first synthesized III-V semiconductors [8]. The crystalline structure of GaN was described in 1937 [9] and growth of GaN crystalline epitaxy layer was developed in 1969 [10]. Three important milestones were reached in 1971. First, Pankov and his partners reported GaN-based metal-insulator semiconductor light emitting diodes (LEDs) [11]. The same year, Manasevit succeeded for the first time to grow GaN with metal-organic chemical vapor deposition (MOCVD) [12]. Last, Dingle and coworkers established the prospect of ultraviolet semiconductor injection lasers via discovering the stimulated light emission from needles of GaN single crystals at a temperature of 2 K [13].

The main obstacle that had to be overcome in making practical nitride-based devices refers to difficulties of growing high-quality AlGaN and InGaN alloys. This is why the nitrides were largely ignored in favor of other wide bandgap materials such as SiC and II-VI materials.

Because lattice-matched substrates are not readily available, mastering epitaxy on foreign substrates is essential to control the chemical purity of GaN and to minimize dislocation in the lattice. The growth of GaN on sapphire substrates resulted in low-quality material full of defects, with a high background free carrier concentration and a rough morphology. In the search for improved properties, Yoshida discovered that an AlN nucleation layer between sapphire substrate and epitaxial layer increases the efficiency of cathodoluminescence of the films [14]. Deposition of a low temperature buffer layer allowed for continuous coverage of the substrate and overcame the wetting obstacles related to surface and interface energetics. Using this AlN low-temperature buffer layer on sapphire substrates, Amano and Akasaki grew the first smooth surface of GaN films in 1986 with MOCVD [15]. This resulted in a significant improvement of the electrical and optical properties of the films. Later, a low-temperature GaN buffer layer was used by Nakamura even more successively [16].

In the same year (1986), Amano demonstrated that silane (SiH_4) could be used as an effective and controllable n-type dopant [15]. Magnesium was supposed to be a good shallow acceptor. Although it was possible to incorporate large amount of Mg in GaN, it did not effectively introduce positive charge carriers (holes) due to unintentional passivation with hydrogen that is present in the MOCVD reactor chamber. This does not occur in MBE systems due to the extremely low H background. In 1989, Amano and Akasaki demonstrated that low-energy electron irradiation activates Mg doped GaN films. With this method they achieved a hole concentration of $10^{16} cm^{-3}$, which was sufficient to produce the first p-n junction-based blue light emitting diode [17]. In 1992, Nakamura reported that sufficiently high hole concentrations could be achieved by thermal annealing of these Mg-doped GaN layers after growth [18]. The development of extremely thin layers composed of InGaN alloys by Nakamura resulted in the realization of a blue LED in 1993 [19].

The next challenge was to a room-temperature nitride laser diode (LD). Although a number of reports on stimulated emission appeared during 1991-1995 [20-23], the goal of an electrically injected device was developed not earlier than the end of 1995 by Nakamura [24]. This achievement induced a rapid improvement in the performance of the lasers. In 1996, Akasaki fabricated a laser diode emitting at a wavelength of 376 nm [25]. In 1998, Nakamura illustrated a room-temperature continuous wave laser emitting at 400 nm [26].

The development of high-power and high-temperature electronics was seen in the last few years. An semiconductor material for power applications should perform excellent transport and thermal properties, a high breakdown voltage, mechanical stability, and allow for the

fabrication of both unipolar and bipolar devices. The III-nitride compounds fulfill most of these demands. In 1993-1994, the first GaN-based transistors were demonstrated [27, 28], but recent developments led to many new exciting achievements. The electron mobility in the two-dimensional electron gas (2DEG) at the GaN/AlGaN interface reaches 10000 cm^2/Vs at cryogenic temperatures and 2000 cm^2/Vs at room temperature [29]. Moreover, a very fruitful combination of high current values (over 20 A/mm) with very high breakdown voltages (several thousand volts) makes the nitrides ideal candidates for high electron mobility transistors [30].

1.2 Application of semiconductors

There is no doubt that semiconductors changed the world beyond anything that could have been imagined before them. The technology of electronics took a large step forward when William Shockley, John Bardeen and Walter Brattain observed the transistor action in a piece of germanium in 1947. They later got the Nobel Prize for this discovery.

The most commonly used semiconductor today is silicon. It is to date the most extensively implemented semiconductor and is widely used in computers, cars and networks. Despite the success of Si devices, the material is not well suited for a wide range of applications, mostly due to its relatively small, indirect bandgap. The search for suitable semiconductor materials led to the development of the compound semiconductors.

Semiconductors based on III-V compound materials provide advance in high-speed microwave and optoelectronic applications. The III-V semiconductors correspond to the compounds formed by the elements in column III (Al, Ga and In) and column V (N, P, As and Sb) in the periodic table. Most of them have the direct bandgaps which means that they can be used to emit light efficiently. Gallium arsenide (GaAs) can be used to make LEDs emit red light. Moreover, due to higher electron mobility, GaAs is widely used in devices requiring high speed such as mobile phones, satellite communications and high frequency radar systems. GaAs devices tend to have less noise than silicon devices. However, the production of GaAs based devices is more costly than devices based on silicon. And the conventional III-V semiconductors (e.g. GaAs, GaP and AlGaAs alloys) together with Si are not suitable for optoelectronic devices in the blue, violet or ultra-violet wavelength regions. The wide band gap semiconductors overcome many of these limitations.

The wide bandgap materials can provide relatively high electron mobility, high thermal conductivity, high breakdown electric fields and thermal and chemical stability [31]. SiC has drawn much attention having a bandgaps around 3 eV. However, due to problems with material quality and device lifetime, only few commercial SiC products exist today such as SiC based metal oxide semiconductor field-effect transistor (MOSFET). The III-nitrides semiconductors are the best candidate materials fulfilling all the requirements for successful

device-making. For instance, the mixture of GaN with In (InGaN) or Al (AlGaN) allows the manufacture of LEDs with colors that can go from green to ultra-violet [32]. GaN based high electron mobility transistors (HEMTs) have found immediate use in various wireless infrastructure applications due to their high efficiency and high voltage operation. GaN based metal semiconductor field effect transistors (MESFETs) and MOSFETs also offer many advantages in high power electronics, especially in automotive and electric car applications [33]. Nanotubes of GaN are proposed for applications in nanoscale electronics, optoelectronics and biochemical-sensing applications [34].

2. Physical properties of III-V semiconductors

The III-V semiconductors have become to the most important materials in the optoelectronics area, due to their specific physical properties mainly due to their wide band gap.

2.1 Crystal structure of III-V Semiconductors

Most semiconductors crystallize in the wurtzite, zincblende and rock-salt structure. Wurtzite can be considered as two interpenetrating hexagonal close-packed lattices having tetrahedral arrangement of four equidistant nearest neighbors. The zincblende structure can be considered as two interpenetrating face-centered cubic lattices, similar to diamond structure but with different atoms in the sublattice. Rock-salt is similar to zincblende but each atom has six nearest neighbors compared with four in the zincblende structure [35]. The crystal structures are shown in Fig. 1.

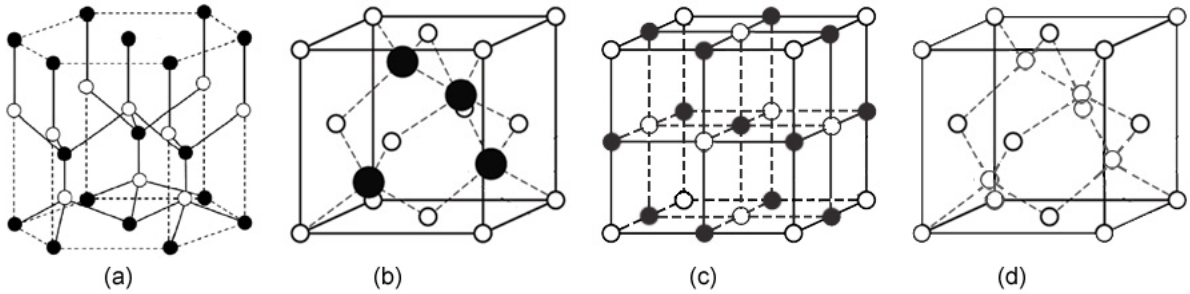

Fig. 1 (a)Wurtzite structure; (b)Zincblende structure; (c)Rock-salt structure; (d)Diamond structure

The III-nitrides crystallize in the wurtzite structure at ambient temperature and pressure. Normally, due to the inherent polarity of crystal structure, there exists a spontaneous polarization and a piezoelectric polarization. In wurtzite GaN, the centers of positive and negative charges from the ionicity of the Ga-N bond are displaced from each other. Therefore electric charges appear at the opposite surfaces of the crystal, which lead to spontaneous polarization. Additional polarization charges result from the physical strain when growing on substrates with different composition and lattice constants (heteroepitaxy). This strain corresponds to the piezoelectric polarization.

2.2 Energy bands of III-V Semiconductors

Figure 2 shows the band gap energies of most III-V semiconductors. All the III-nitrides have direct band gap, implying direct transition at the Γ point in the **E·k** diagram (Fig. 3). The band gap energies of III-nitrides span a wide range from 0.7 eV (InN) over 3.4 eV (GaN) to 6.2 eV (AlN), covering infra-red and ultra-violet spectral ranges as well as the visible range. And the in-plane lattice constant *a,* is 0.31 nm for AlN and to 0.36nm for InN.

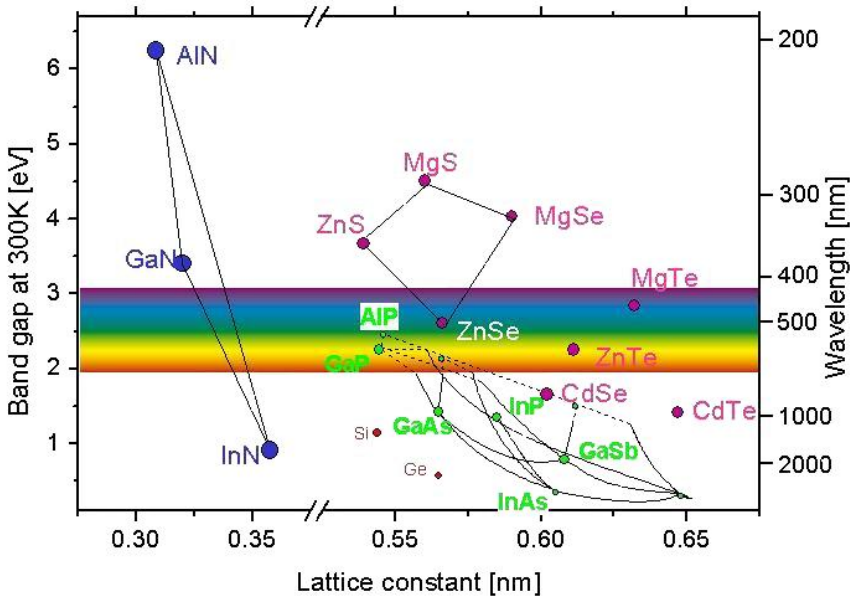

Fig. 2 Band gap energies of most III-V Semiconductors with respect to the lattice constant [36]

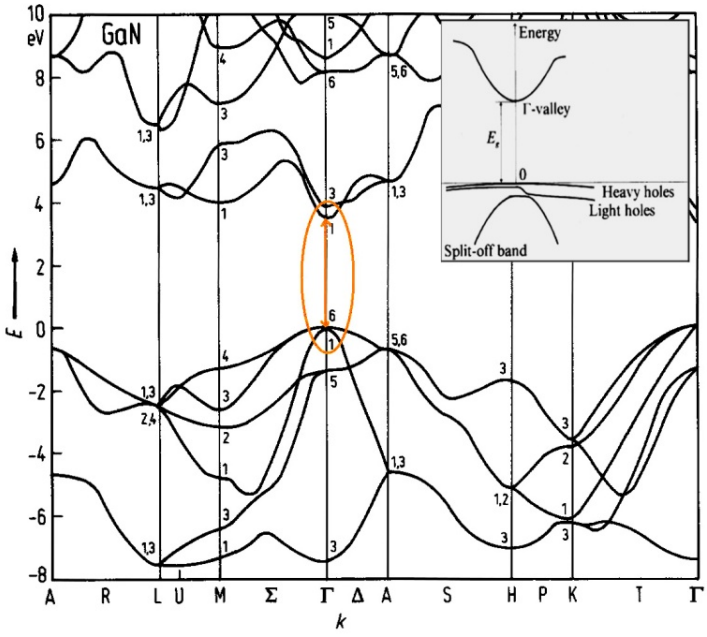

Fig.3 Band gap structure of GaN

The electronic band structure for GaN is displayed in Fig. 3. GaN is a direct band gap compound semiconductor with its highest energy point in the valance band and its lowest energy point in the conduction band located in the same point, Γ, in the k-space. In a wurtzite crystal, the $|Z\rangle$ state (corresponding to the p_z state) becomes unique because of the crystal field generated by the wurtzite structure, whereas the other two states $|X\rangle$ and $|Y\rangle$ (corresponding to the p_x and p_y states) are degenerate. The $|Z\rangle$ state forms a subband called the split-off band with an

energy difference of approximately 10 meV. The states $|X + iY, \uparrow\rangle$ and $|X - iY, \downarrow\rangle$ have parallel magnetic moments from orbiting electrons and electron spin and therefore form heavy holes. The states $|X + iY, \downarrow\rangle$ and $|X - iY, \uparrow\rangle$ have antiparallel magnetic moments forming light holes, which are about 17 meV lower in energy compared to the heavy holes [37].

2.3 Schottky and Ohmic contact of III-V Semiconductors

Metal-semiconductor contacts are categorized into Schottky contacts (rectifying) and Ohmic contacts (non-rectifying). The Schottky contact allows conduction of the current only under forward bias conditions. An ohmic contact, as the name indicates follows Ohm's Law. Current flowing through an ohmic contact is the linear function of the applied voltage and conduction is possible under both forward and reverse bias.

2.3.1 Principle of Schottky contact

When a metal is sputtered or evaporated onto a semiconductor surface, a Schottky contact is formed. The magnitude of the band bending in both n-type and p-type semiconductor is displayed in Fig. 4 which also describes the operation of the Schottky contact.

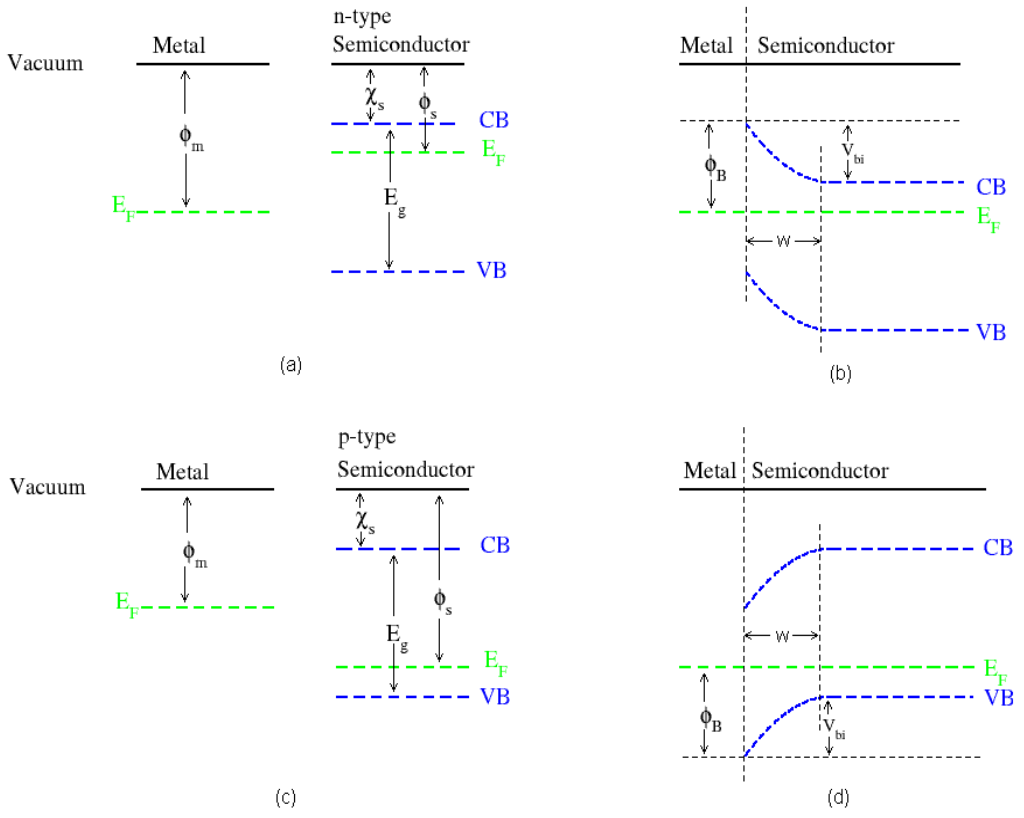

Fig. 4 Ideal diagram of metal n-type Schottky contact: (a) before contact; (b) after contact; Ideal diagram of metal p-type Schottky contact: (c) before contact; (d) after contact [38].

In Fig. 4, ϕ_B is the potential barrier and V_{bi} is the built-in voltage. The difference between the Fermi level and vacuum level is termed the work function, ϕ_m and ϕ_s for metal and semiconductor respectively. In the n-type case where $\phi_m > \phi_s$, electrons flow from the semiconductor with lower work function but higher energy states to the metal until the Fermi level aligned to achieve the thermal equilibrium [38]. In the p-type case, electrons flow from the metal to the semiconductor until equilibrium (and corresponding barrier) is reached.

2.3.2 Principle of Ohmic contact

The basic principle of ohmic contact is similar to the principle of Schottky contact. Electrons flow from the lower work function of the semiconductor/metal combination to the higher work function of metal/semiconductor. However, an ohmic contact only forms when the resistance within the contact is negligibly small compared to the resistance of the semiconductor. The most important difference between the Schottky contact and ohmic contact is the width of the depletion region w.

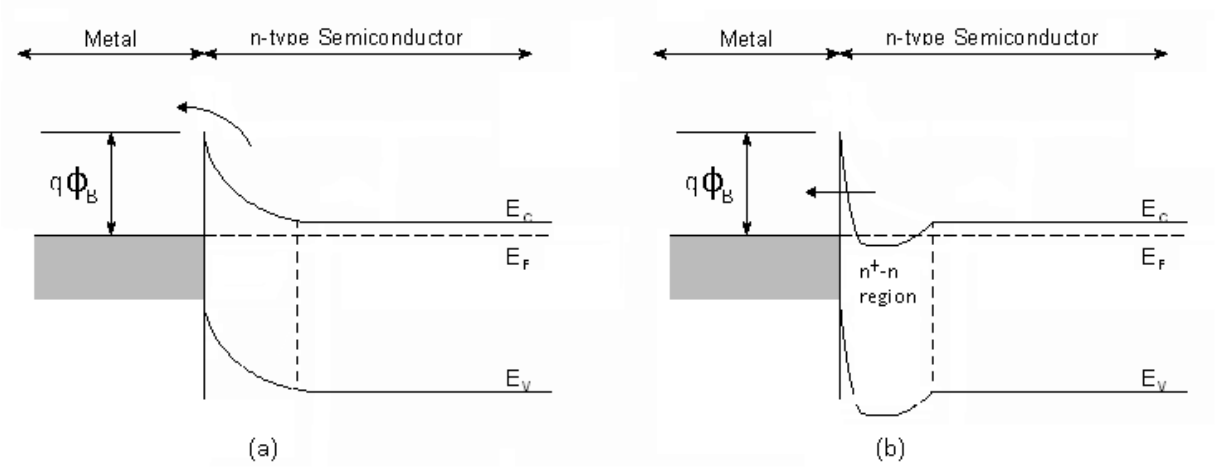

Fig.5 (a) Lower barrier height of Ohmic contact in n-type semiconductor;
(b) Ohmic contact after high doping in n-type semiconductor. [39]

From Fig. 5(a), we see that moving up the Fermi level results in a lower potential barrier ϕ_B and lower built-in voltage V_{bi}. In this case, electrons can jump over the barrier. Moreover, the barrier height also decreases due to the image force lowering effect. When an electron from the semiconductor side approaches the metal-semiconductor interface, a positive charge is created at the metal surface due to the repulsion of the negative charges. Image force is defined as an attractive force between the positive charge and the electron [40].

A common way of employing the process image force lowering effect is to increase the carrier concentration. This can be achieved by through heavy doping of the semiconductor. It is also a method used commonly to reduce the thickness of depletion region. However, it is difficult to

make ohmic contacts on wide band gap semiconductors. In such cases the general technique is to heavily dope the surface layer to produce an n^+- region near the surface to form an n^+-n junction [39]. In this case, tunneling will dominate the current transport and the barrier becomes transparent to electrons in both directions displayed in figure 5(b).

2.3.3 Ohmic contact for GaN

For the formation of high-quality ohmic contacts to GaN, the contacts should have a low Schottky barrier or the GaN needs to be heavily doped to allow carriers to tunnel through the barrier. Because the height of Schottky barrier depends on the work function of contact metals, for n-type GaN, ohmic contacts can be easily formed by using metals having a work function ϕ_m that is smaller than that of n-GaN, e.g. In (ϕ_m=4.12 eV), Al (ϕ_m=4.28 eV) and Ti (ϕ_m=4.33 eV) [41]. For these contacts to n-GaN with a carrier concentration of $5 - 7 \times 10^{18} cm^{-3}$, low contact resistances range from 10^{-5} to $10^{-8}\ \Omega \cdot cm^2$. These resistances are low enough for good ohmic contacts and thus for the operation of optoelectronic and electronic devices [42].

In contrast, to produce ohmic contacts to p-type GaN one needs is to use metals having a larger work function. However, it is difficult to form good-quality ohmic contacts with a specific contact resistance that is lower than $10^{-4}\ \Omega \cdot cm^2$. This is mainly due to the high activation energy of the deep Mg acceptors (134 meV) [43]. Ni/Au contact has been commonly used to form the ohmic contacts to p-GaN because Ni has large work function ϕ_m=5.15 eV. Ni/Au contacts generally produce a specific contact resistance of $10^{-2}\ \Omega \cdot cm^2$ [44]. Annealing the Ni/Au contacts in ambient at 500 °C results in a specific contact resistance in the range of $10^{-4} - 10^{-6} \Omega \cdot cm^2$[45].

3. Impurities in III-V semiconductors

3.1 Shallow impurities

Shallow impurities are defined as impurities which are ionized at room temperature (25 meV). Shallow impurities, which determine the conductivity and the carrier type of the semiconductor, can be either acceptors or donors. A donor has an extra electron that can be excited from the dopant to the conduction band, while an acceptor accepts electrons excited from the valence band thereby leaving a hole behind.

3.2 Bohr's hydrogen atom model

When an extra charge provided by a doping atom move through the lattice, it will be attracted by a weak potential at the ionized impurity atom. This electrostatic potential of a point charge is the so called Coulomb potential. The Coulomb potential of a positive point charge (+e) in vacuum located at r is obtained from Poisson's equation and is given in spherical coordinates by [46]

$$V(r) = \frac{e}{4\pi\varepsilon_0 r} \tag{3.1}$$

where ε_0 is the permittivity of vacuum. When this is compared to the central symmetric potential, or the physical system of a charge and an ionized centre, it is seen that it can be described by Bohr's hydrogen model. For the Bohr hydrogen atom model, to simultaneously meet the conditions of a stationary circular motion of the electron around the proton and the quantization of the angular momentum of the electron, we introduce the Bohr radius (n=1) and the kinetic energy

$$a_{B,n} = \frac{4\pi\varepsilon_0 n^2\hbar^2}{m_0 e^2} \qquad \text{(n=1,2,3...)} \tag{3.2}$$

$$E_{kin,n} = \frac{1}{2}m_0 v^2 = \frac{1}{2}\frac{1}{(4\pi\varepsilon_0)^2}\frac{e^4 m_0}{n^2\hbar^2} \qquad \text{(n=1,2,3...)} \tag{3.3}$$

This energy represents the energy required to remove the electron from the energy state *n* to an infinite distance from the proton. For n=1, an energy E_{kin}=13.6eV is required to ionize a hydrogen atom [47].

3.3 Hydrogen-like donors and acceptors

The hydrogen atom model can be applied to shallow donors ($E_{Si,d} = 5.8\,meV$) in III-V Semiconductors. Such donors are called hydrogen-like donors. Effective Bohr radius and ionization energy are well predicted for such donors. In order to apply the model for dopants in semiconductors, we need to know the effective mass of carriers m_e^* and the dielectric constant ε of the semiconductor. Using these two parameters, the following properties of hydrogen-like impurities can be derived.

$$a_{B,n}^{*} = \frac{4\pi\varepsilon n^2\hbar^2}{m_e^{*}e^2} \qquad \text{(n=1,2,3…)} \tag{3.4}$$

$$E_{kin,n}^{*} = \frac{1}{2}\frac{1}{(4\pi\varepsilon)^2}\frac{e^4 m_e^{*}}{n^2\hbar^2} \qquad \text{(n=1,2,3…)} \tag{3.5}$$

For ground state n=1, we get the donor Bohr radius a_B^{*} and the donor ionization energy as

$$a_B^{*} = \frac{4\pi\varepsilon\hbar^2}{m_e^{*}e^2} = \frac{\varepsilon_r}{m_e^{*}/m_0}a_B = \frac{\varepsilon_r}{m_e^{*}/m_0}0.53\text{Å} \tag{3.6}$$

$$E_B = \frac{e^4 m_e^{*}}{2(4\pi\varepsilon\hbar)^2} = \frac{m_e^{*}/m_0}{\varepsilon_r^2}E_{kin} = \frac{m_e^{*}/m_0}{\varepsilon_r^2}13.6eV \tag{3.7}$$

where ε_r is static dielectric constant ($\varepsilon_r = {}^{\varepsilon}/_{\varepsilon_0}$, ε_0 is the permittivity of vacuum) and m_0 is the free electron mass. The ground state energy E_B means the ionization energy from the first energy state to the band edge of the shallow impurity [47].

Application of the hydrogen atom model to acceptors in III-V Semiconductors is more complicated due to their degenerate valence band structure. In 1973, Baldareschi and Lipari developed a now widely accepted model for shallow acceptor stated in cubic semiconductors with degenerate valence bands [47]. According to their calculation,

$$a_B^{*} = \frac{4\pi\varepsilon\hbar^2\gamma_1}{m_h^{*}e^2} \tag{3.10}$$

$$E_B = \frac{e^4 m_h^{*}}{2(4\pi\varepsilon\hbar)^2\gamma_1}f(\mu) \tag{3.11}$$

where the parameter γ_1 is the so-called Luttinger parameter. And $f(\mu)$ is a function that relates the acceptor ionization energy with the effective kinetic energy.

The effective mass and dielectric constant in GaAs and GaN is presented in Table 1. These values were used to calculate the energy levels of a few donor and acceptor impurities in GaAs and GaN (Table 2) according to the hydrogen model.

Table 1. Effective mass of electrons and holes and dielectric constant of GaAs and GaN. Listed are the electron effective mass m_e^*, the heavy hole effective mass m_{hh}^*, the light hole effective mass m_{lh}^* and the dielectric constant ε_r [48].

Material	$\boldsymbol{m_e^*}$	$\boldsymbol{m_{hh}^*}$	$\boldsymbol{m_{lh}^*}$	$\boldsymbol{\varepsilon_r}$
GaAs	0.067	0.45	0.082	13.1
GaN	0.15-0.21	0.6	0.26	9.0

Table 2. Shallow energy levels for GaAs and GaN and impurities [49].

Material	**Donors**	**Energy (meV)**	**Acceptors**	**Energy (meV)**
GaAs	Si	5.8	Mg	28
	Ge	6.0	Si	35
	S	6.0	Be	28
	Sn	6.0	C	26
GaN	Si	25-35	Mg	134

4. The Hall Effect

In 1879, E. H. Hall first discovered that an electromotive force may be generated across a current-carrying conductor by placing the conductor in a magnetic field [50].This phenomenon attracted much interest over the years and it is well known as the Hall effect today.

4.1 The Hall effect principle

When an applied magnetic field is perpendicular to the direction of the current flow, a voltage will be developed across the Hall element and is referred as the Hall voltage. The basic geometry for the Hall Effect is shown in Fig. 6.

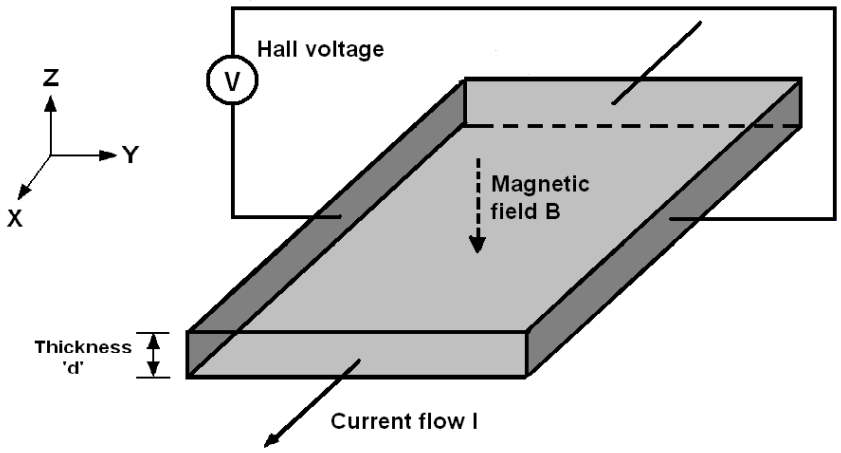

Fig. 6 Hall element showing critical dimensions and reference axes

The basic principle underlying the Hall effect is the Lorentz force [51]. With expresses the force on a point charge due to an applied electromagnetic fields.

$$\boldsymbol{F} = e[\boldsymbol{E} + \boldsymbol{v} \times \boldsymbol{B}] \tag{4.1}$$

where **v** is the velocity of the charge carriers and, **E** and **B** are the electric field and magnetic field intensity respectively.

Steady state is achieved when $F_y = 0$, which reflects that the electric field produced by the carrier concentration gradient neutralizes the magnetic deflection given as

$$eE_y - ev_x B_z = 0 \tag{4.2}$$

According to the expression of current density [52]

$$J_x = \sum_i n_i \, e v_x^{(i)} \tag{4.3}$$

if we assume that all the carriers have the same velocity, we obtain

$$J_x = nev_x \text{ , where } n = \sum_i n_i. \tag{4.4}$$

Related to the Eq. (4.2), E_y can be written as

$$E_y = \frac{J_x B_z}{ne} \tag{4.5}$$

The Hall coefficient is defined as

$$R_H \equiv \frac{E_y}{J_x B_z} = \frac{1}{ne} \tag{4.6}$$

From Eq. (4.6), we see that the Hall coefficient is inversely proportional to the carrier concentration, n, and also demonstrates the type of the carriers, negative for electrons while positive for holes [51].

4.2 The Hall Effect in semiconductors

Hall Effect in semiconductors where there are both electrons and holes involves not only the concentrations of electrons and holes, n and p respectively, but also the electron and hole drift mobilities, μ_e and μ_h[53].

Considering a single carrier acting in the net electrostatic force $F_{net} = \pm eE$, based on the relationship between drift velocity and mobility, we acquire

For holes $$v_h = \mu_h E = \mu_h \frac{F_{net}}{e}$$

For electron $$v_e = \mu_e E = -\mu_e \frac{F_{net}}{e} \tag{4.7}$$

At steady state, there is no net current along the y-direction.

$$F_{hy} = eE_y - ev_{hx}B_z \quad \text{and} \quad -F_{ey} = eE_y + ev_{hx}B_z \tag{4.8}$$

$$J_y = J_h + J_e = epv_{hy} + envey = 0 \tag{4.9}$$

From Eq. (4.7), we have

$$F_{hy} = \frac{ev_{hy}}{\mu_h} \quad \text{and} \quad -F_{ey} = \frac{ev_{ey}}{\mu_e} \tag{4.10}$$

Substituting $v_{hx,ex} = \mu_{h,e}E_x$ and Eq. (4.10) into Eq. (4.8)

$$\frac{v_{hy}}{\mu_h} = E_y - \mu_h E_x B_z \quad \text{and} \quad \frac{v_{ey}}{\mu_e} = E_y + \mu_e E_x B_z \tag{4.11}$$

From Eq. (4.9), we get $pv_{hy} = -nv_{ey}$ which we substitute to Eq. (4.11)

$$E_y(p\mu_h - n\mu_e) = E_x B_z(p\mu_h^2 - n\mu_e^2) \tag{4.12}$$

The current along the x-direction is given by

$$J_x = J_h + J_e = epv_{hx} + env_{ex} = ep\mu_h E_x + en\mu_e E_x \tag{4.13}$$

If we combine the expression with Eq. (4.12), we obtain the Hall coefficient

$$R_H = \frac{p\mu_h^2 - n\mu_e^2}{e(p\mu_h + n\mu_e)^2} \tag{4.14}$$

From Eq. (4.14), we can conclude that the Hall coefficient in semiconductors depends on both concentration and mobility of electrons and holes. When $p\mu_h^2 - n\mu_e^2 > 0$, R_H will be positive, and vice versa.

4.3 The Hall Effect measurement

Virtually every major semiconductor laboratory makes use of the Hall effect to measure the carrier concentration and to determine the polarity. The method is simple and yields carrier concentration n (or p), mobility μ and resistivity ρ. The expressions used to measure and calculate them are briefly stated below [54].

$$V_H = \frac{I \cdot B}{ned} \tag{4.15}$$

$$\mu = \frac{1}{ne\rho} \tag{4.16}$$

Where V_H is the Hall voltage, B the magnetic field strength, I the current passing through the sample and d is the thickness of the sample layer.

4.3.1 Van der Pauw structures

The Van der Pauw measurement geometry became the most popular Hall effect measurement configuration after Van Der Pauw solved the potential problem in a thin layer of arbitrary shape in 1958. While the primary conditions demand the sample to be flat, homogenous and isotropic, the most difficult part to realize the van der Pauw technique is to make true ohmic contacts on the surface.

Although arbitrary shape is applicable, in practice a symmetrical shape is preferable because of the ease of the fabrication. Some of the more common examples are displayed in Fig. 7. Consider the configuration displayed in Fig. 7(a), with a square sample with triangular contacts at the corners of the square. This shape, perhaps the most common in use today, is also the geometry used in our measurements. Unfortunately, the square shape is more sensitive to the finite-contact-size problem as compared with other configurations. In Fig. 7, l_c is the length of the contact points and l_s is the sample length.

Generally, l_c/l_s is supposed to be less than 0.1. According to Fig. 8(a) and Fig. 8(b), the uncertainty of the resistivity for this value will be less than 0.7% and the deviation from the theoretical Hall voltage will be ~6%. In our laboratory, the sample is cut into size between $3 \times 3\ mm^2$and $4 \times 4\ mm^2$ with a contact size of 0.5 mm. Thus, $\frac{l_c}{l_s} \approx 0.125 - 0.16$. The resistivity correction factor is therefore 2%. While the Hall voltage correction factor is 10%—15%. According to Eq. (4.15) and Eq. (4.16), the correction factor for carrier concentration and mobility is calculated as 17% and 2% respectively. Thus, a sample with a longer periphery and smaller contact is preferred for Hall effect measurement.

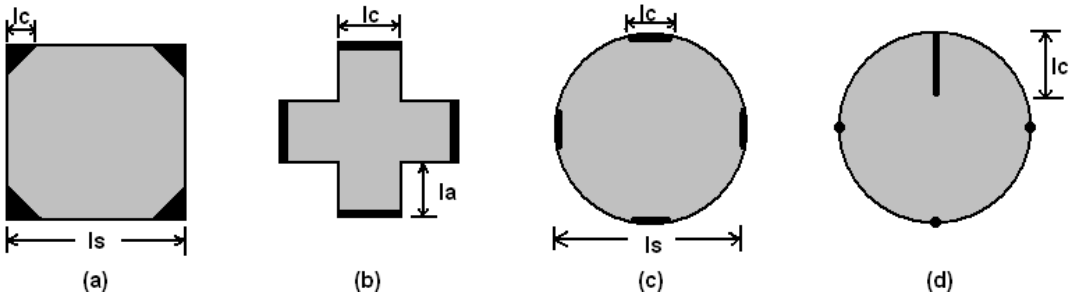

Fig. 7 Various Van der Pauw structures with finite contact size: (a) square; (b) Greek cross; (c) and (d) circles.

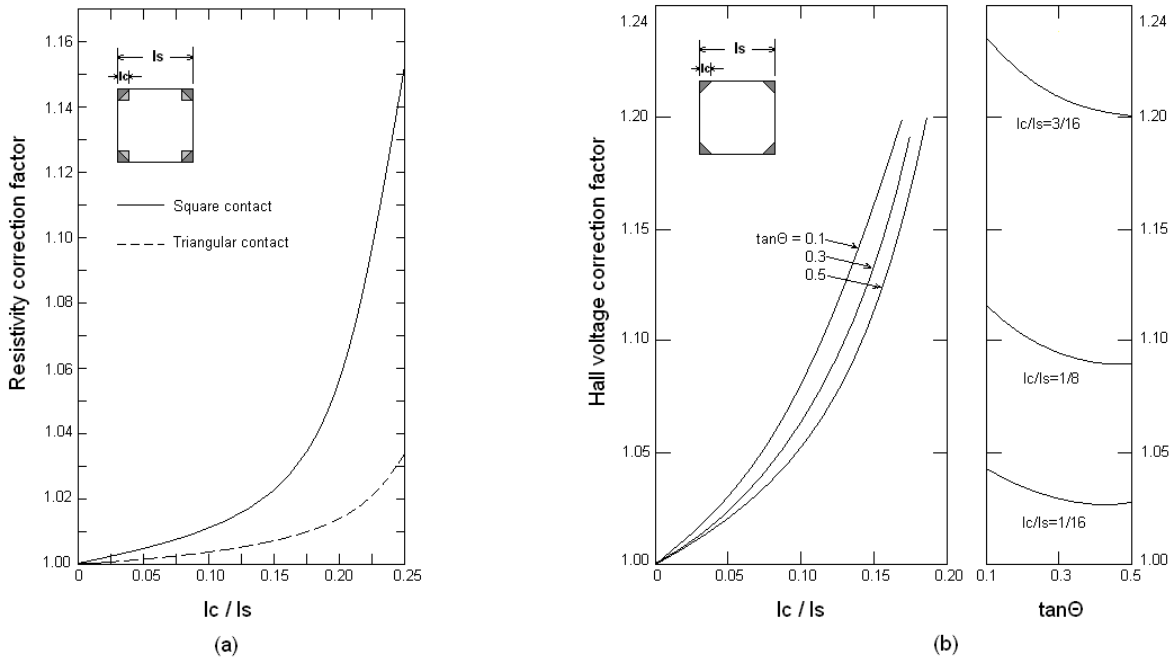

Fig. 8 (a) Contact-size correction factors for the resistivity of a square pattern; (b) Contact-size correction factors for the Hall voltage of a square pattern. Here Θ is the Hall angle, defined as $tan\theta = -\frac{E_x}{E_y} \approx -\mu B$ [55].

4.3.2 Measurement method and errors analysis

As discussed before in Eq. (4.15) and Eq. (4.16), we can calculate the mobility and carrier concentration by measuring the value of Hall voltage and resistivity. Consider the sample with the square shape shown in Fig. 9.

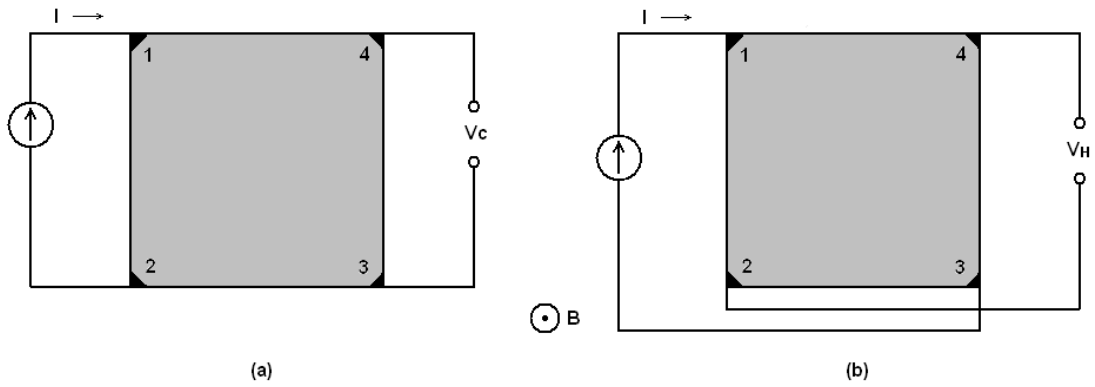

Fig. 9 A square shape for van der Pauw measurements: (a) resistivity; (b) Hall Effect.

In Fig. 9(a), a current I flows from contact 2 to 1, and a voltage Vc is measured between contact 3 and 4. We define the resistance $R_{ij,kl} \equiv V_{kl}/I_{ij}$, where the current enters contacts i and leaves contact j, and voltage is measured from contact k to contact l. Thus without the magnetic field, the resistivity ρ is written as follows:

$$\rho = \frac{\pi d}{ln2}\left[\frac{R_{21,34}+R_{32,41}}{2}\right] f \tag{4.17}$$

where f is determined from the transcendental equation:

$$\frac{Q-1}{Q+1} = \frac{f}{ln2} arccosh\left\{\frac{1}{2} exp\left[\frac{ln2}{f}\right]\right\} \tag{4.18}$$

and Q is the resistivity-ratio calculated as $R_{21,34}/R_{32,41}$ and should be >1, otherwise it should be inversed. By solving the equation system:

$$Q = \frac{\ln\left(\frac{1}{2}-\alpha\right)}{\ln\left(\frac{1}{2}+\alpha\right)} \tag{4.19}$$

$$f = \frac{\ln\left(\frac{1}{4}\right)}{\ln\left(\frac{1}{2}+\alpha\right)+\ln\left(\frac{1}{2}-\alpha\right)} \tag{4.20}$$

we can also get the value of f by first calculating α as a function of Q.

Furthermore, to average the resistivity ρ, we need to include two other contact permutations and also need to reverse the current for all four permutations. Then we obtain

$$\rho = \frac{\pi d}{ln2} \cdot \frac{1}{8}\left[(R_{21,34} - R_{12,34} + R_{32,41} - R_{23,41})f_A + (R_{43,12} - R_{34,12} + R_{14,23} - R_{41,23})f_B\right]$$

(4.21)

where f_A and f_B are determined from Q_A and Q_B respectively [56].

Measuring the Hall voltage V_H is theoretically straightforward according to Fig. 9(b). However, in real measurements, the extraction of the Hall voltage is by various undesired effects such as [57]:

(1) The potential difference caused by the Etinghausen effect. All electrons moving along the negative y-axis do not have the same velocity **v**. Electrons with higher speed induce larger radius of gyration which make them reach one side of the semiconductor quickly. More electrons with higher energy accumulate on one side than the other side. It arises a temperature difference between two sides generating the potential difference U_E.

(2) The potential difference caused by Nernst effect. The resistivity within each contact point is different. When the current goes through them, contacts get heated, giving rise to thermal diffusion current. Similar to Hall Effect, this thermal diffusion current will generate a potential difference U_N.

(3) The potential difference caused by Righi-Leduc effect. According to the Etinghausen effect which arises from the different velocities of thermal diffusion electrons, another kind of thermal electromotive potential U_R is generated between the contacts.

(4) Due to manufacturing difficulties and the heterogeneity of the material, even without external magnetic field, there will be a potential difference when the current goes through it.

Molecular beam epitaxy

Molecular beam epitaxy (MBE) is a technique for epitaxial growth that occurs on a heated crystalline substrate surface. Epitaxy is described as the controlled deposition of one crystal upon another crystal. This process produces very pure materials. In addition, it offers the advantage of changing growth material within a few atomic layers, suitable for growth of heterostructures.

The term epitaxy is constituted of the Greek words *epi* meaning "on" and *taxis* meaning "ordered", and was coined by Royer in 1928. Royer put forward several rules for the occurrence of epitaxy, the most important of which can be written as [58]:

- There must be a matching of symmetry between the contacting crystal planes of the substrate and overgrowth.
- The misfit between parallel lattice rows at the interface must be less than 15%.

Today, epitaxy is used in the commercial production of light emitting diodes, laser diodes and high frequency transistors. Ideally, epitaxy should take place on a lattice matched substrate i.e. where the growth material is the same as the initial substrate, also known as homoepitaxy, or when the semiconductor is perfectly matched to a substrate of another material, referred to as lattice-matched heteroepitaxy. The samples presented in this thesis were all produced by MBE.

5.1 General description of the MBE system

MBE growth of semiconductors takes place in an ultra-high vacuum (UHV) environment. In Fig.10 a schematic of a typical MBE system is shown. The solid sources materials such as Ga are placed in effusion cells to provide an angular distribution of atoms or molecules in a beam, which hits the surface of a single crystalline substrate. The substrate is heated to the necessary temperature and is continuously rotated to improve the homogeneity of growth.

To reach the molecular beam conditions, the mean free path λ of the particles should be larger than the geometrical size of the chamber. This is fulfilled if the total pressure is below 10^{-5} torr. However, for growing a sufficiently clean epitaxial layer or epilayer, a typical gallium flux is 10^{19} atoms m^{-2} s^{-1} corresponding to a growth rate of 0.5-1µm/h, the background or base pressure should not exceed 10^{-11} torr. This is concluded from the requirement that the monolayer deposition times of the beams t_b and the back ground residual vapor pressure t_{res} should fit the equation $t_{res} < 10^{-5} t_b$ [59]. Therefore, UHV is essential for MBE systems. Pyrolytic boron nitride is chosen for the crucibles which are thermally stable up to 1400°C. Refractory metals such as molybdenum and tantalum are widely used for the shutters, the heaters and other components. In addition, only ultrapure materials can be used as sources [59].

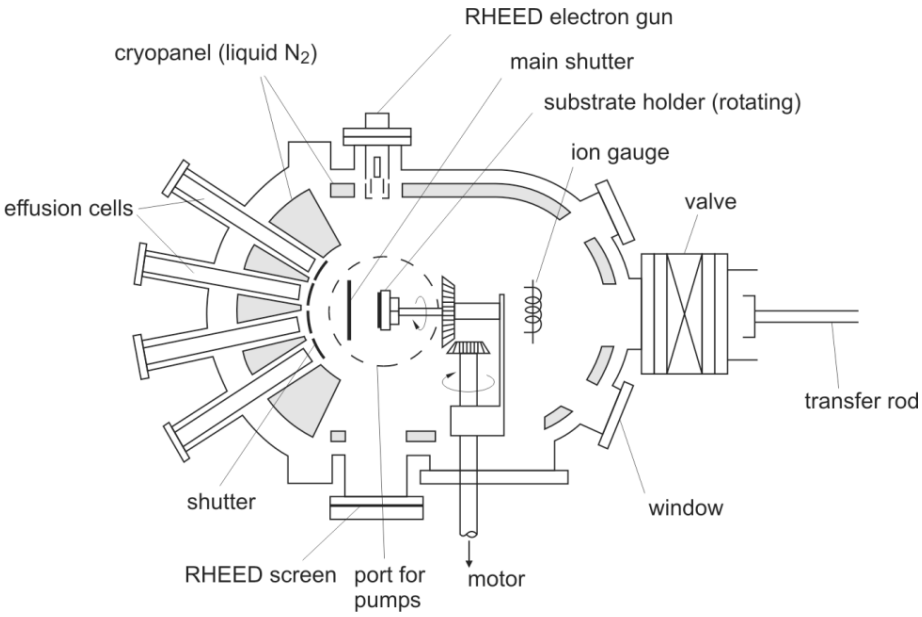

Fig. 10 A typical MBE system [60].

MBE systems permits the control of composition and doping of growing structures at the monolayer level by changing the nature of the incoming beam just by opening and closing mechanical shutters. The UHV environment of the system is also important for the operation of reflection high energy electron diffraction (RHEED). The RHEED shows the diffraction from the sample surface in real time and gives direct information on the state of the surface. RHEED oscillations (Fig. 11) accurately yield the growth rate during the growth of GaAs layer [61]. Unfortunately, due to the specific growth conditions for nitrides, RHEED oscillations are only observable during suboptimal growth conditions for nitride layers.

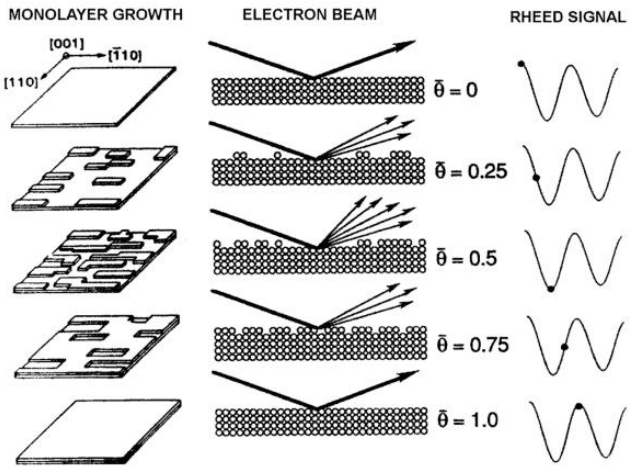

Fig. 11 Intensity oscillations of the specular beam in the RHEED pattern from a surface. The period corresponds to the growth rate of exactly a monolayer [62].

5.2 Epitaxial growth of III-nitrides

For III-nitrides growth, there are two dominating epitaxial technologies, MBE and metal-organic vapor phase epitaxy (MOVPE). The greatest problem concerning III-nitrides epitaxy growth is the lack of an inexpensive, sufficiently large ($\geq 1cm^2$) and lattice-matched substrate of sufficiently high quality.

5.2.1 Substrate for GaN growth

Choosing a proper substrate is an important task for growing GaN crystal film of good quality. Due to high melting point of GaN and the high vapor pressure, it is difficult and costly to fabricate a GaN substrate [63]. Therefore, heteroepitaxy is usually employed for growing GaN-based materials. Table 3 lists the disadvantages related to heteroepitaxy of GaN.

Table 3. Challenges commonly encountered with heteroepitaxy [64].

Substrate property	Consequence for a substrate
Lateral mismatch of lattices	High-tension leakage currents of an unit due to high density of dislocations; short life times of minority charge carriers; decrease in specific thermal conductivity; accelerated diffusion of impurities
Vertical mismatch of lattices	Counter-phase interfaces; boundaries of inversion domains
Surface steps in non-isomorphous substrates	Mismatch boundaries of packing
Discrepancy between thermal conductivity coefficients	Strain thermally induced in a film
Low thermal conductivity coefficient	Weak dissipation of heat
Difference in chemical composition as compared to that of an epitaxial film	Contamination of film with substrate elements; boundary electronic stales made by broken bonds; poor wetting of a substrate with growing film

Using a foreign substrate for nitride growth, a number of factors such as crystal orientation, polarity and concentration of defects of the epitaxial film will be effected. A detailed review of different substrates for GaN growth was made by Liu *et al* [64].

Researchers have also developed homoepitaxial substrates, but the process still needs some improvements. Several substrates are compared in Table 4 [64].

Table 4 Display the properties of several different substrates. Listed are the crystal structure, lattice constant, thermal conductivity and thermal expansion coefficient [64].

Substrate Material	Crystal structure	Lattice Constant (nm)	Thermal conductivity (W/cm·K)	Thermal expansion coefficient (10^6 K) a-,c-axis
GaN	Hexagonal	a=0.318843 c=0.518524	2.1	5.59,6.30
Sapphire	Hexagonal	a=0.4765 c=1.2982	0.23~0.25	7.5,4.33
6H-Silicon carbide	Hexagonal	a=0.30806 c=1.51173	3.6-4.9	4.46,4.16
Silicon	Cubic	a=0.543102	1.56	2.59
γ-Lithium aluminate ($LiAlO_2$)	Tetragonal	a=0.5169 c=0.6267	2.83	7.1,15

5.2.2 Growth of III-nitride layer

For III-nitrides materials, the material quality is highly sensitive to the growth conditions. Growth temperature influences the growth of GaN, AlN and InN by varying the incorporation rate, desorption rate and thermal decomposition. Typically, GaN and AlN have 1µm/h decomposition rates at 850 °C [65] and 1400 °C [66] respectively. MBE growth of GaN most often takes place at $T_s = 700 - 750°C$. When the temperature is reduced, a deterioration of material quality is often observed due to lower surface atom mobility. A key parameter for III-nitride growth is the III-V ratio. For GaN, when increasing the III-V ratio to >>1, the growth conditions go from nitrogen rich to gallium rich. Nitrogen-rich surface gives material with rough surfaces and poor crystalline quality. A Ga-rich surface shows Ga droplets forming on the surface and these also have a negative effect on the layer properties [67]. Optimum growth conditions are reached under Ga-stable (slightly Ga-rich) conditions giving smooth surfaces, higher crystal quality and better optical and electrical properties.

6. Experiments

6.1 Hall Effect Setup

The Hall Effect setup includes three main parts: Sample holder, electronic control and computer program. Figure 12 shows the Hall Effect setup in the MBE lab.

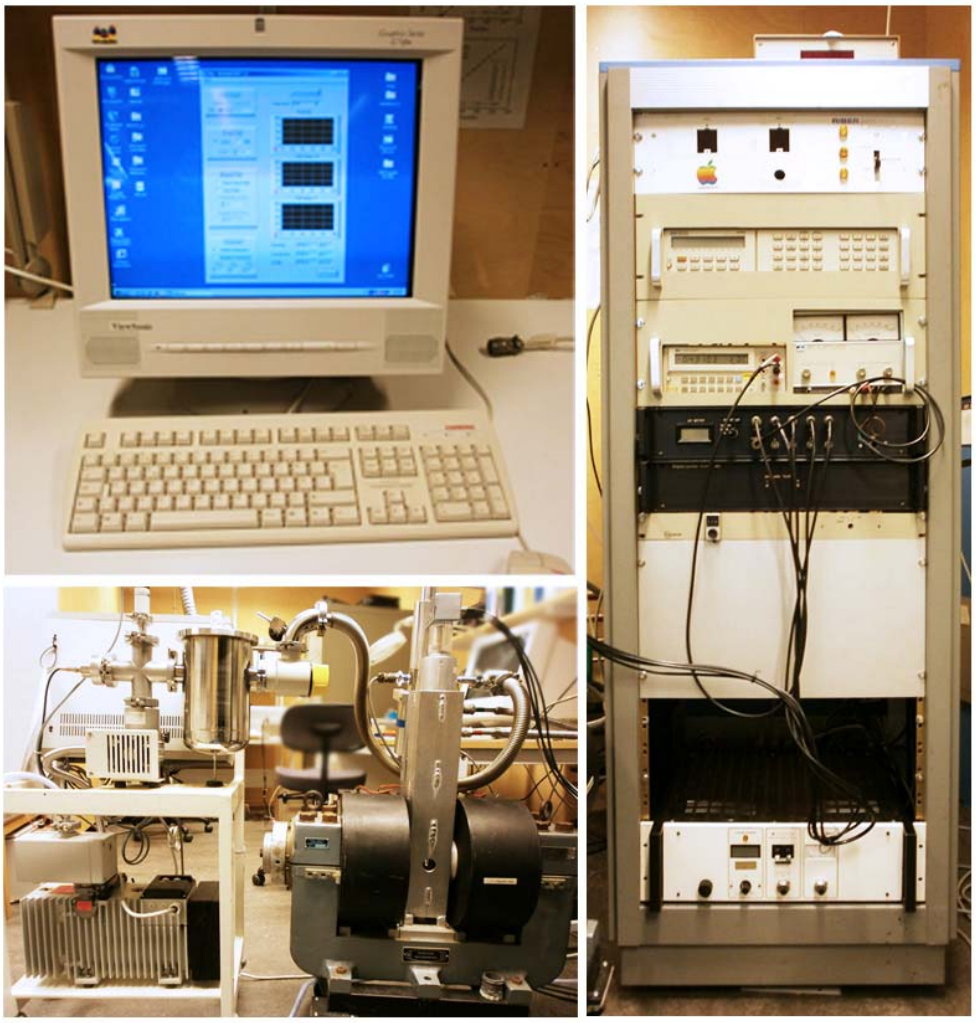

Fig.12 The Hall Effect setup in the MBE lab

In Fig. 12, to the upper left is the lab computer which runs the Hall Effect program and data processing shown. In the left-bottom picture, the turbo pump is shown. This pump can pump the system to 10^{-9} torr. It is connected to the cryo sample holder. This can be used to do temperature dependent Hall Effect measurements. To the right of the pump, the two black cylindrical objects are the electromagnets. The holder is inserted between these magnets during measurement. To the right in Fig. 12, several different electronic instruments used to control the system are arranged into a rack. These instruments are connected to each other according to the schematic shown in Fig. 13.

Figure 13 shows the outline of the backside of the system control rack (right picture in Fig. 12).

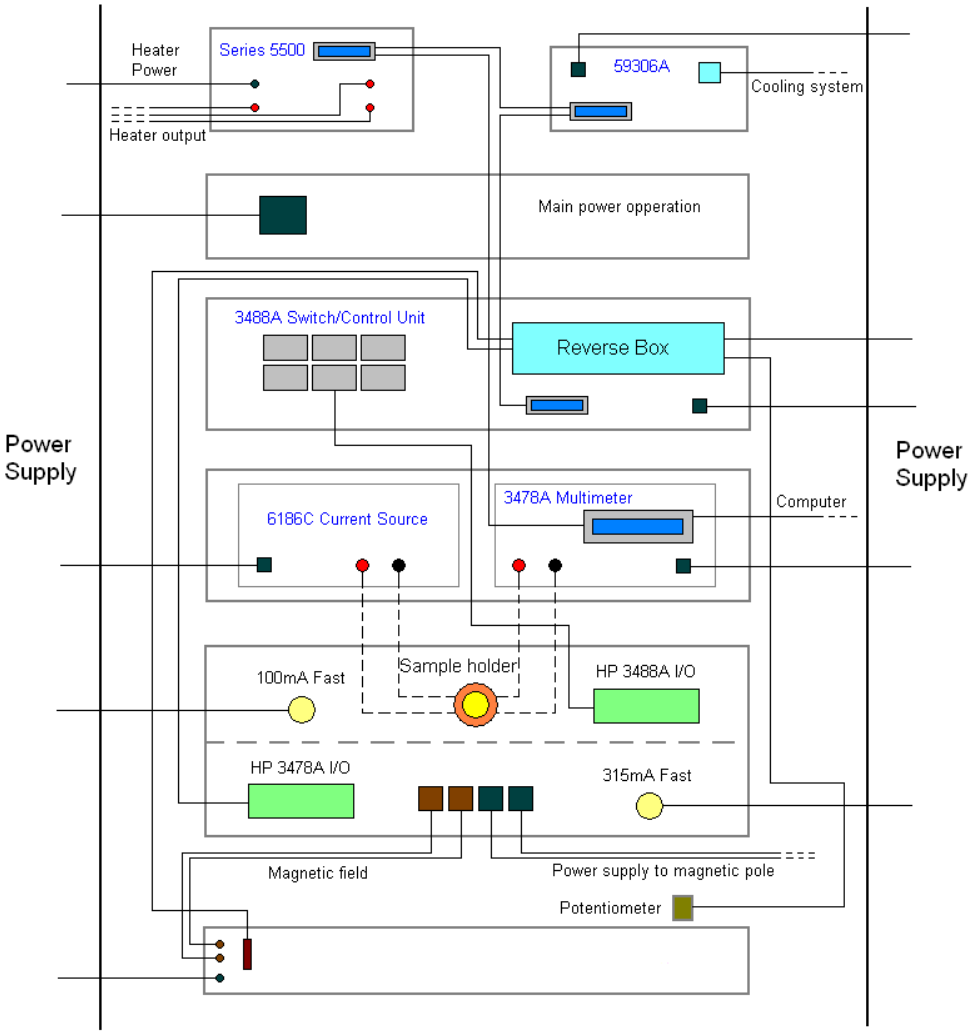

Fig. 13 Schematic of the Hall Effect system control rack.

The series 5500 is employed to control the temperature and output the temperature value. The 59306A unit is applied to cool the cryo sample holder and give feedback on the temperature. The 3488A device can be referred as the core instrument which switches the operation of the multimeter, power supplies, signal analyzers and other instruments. All units are controlled by a computer program. The 6186A is a current source while 3478A is a voltage source. Both of them transfer the signal data to the HP 3478A I/O from the front side of the frame. The 3478A is sensitive enough to measure the extremely small voltages and currents. Voltage, current, resistivity and temperature will be transferred into the computer program through 3478A. A potentiometer is used to change magnetic field strength. Using a magnetic probe, we tested the magnetic field strength with change of the potentiometer to calibrate the magnetic field.

First, we checked the stability and the degree of accuracy of the magnetic system. The magnetic field strength was measured along axes via varying the distance from the zero point "O" to both negative and positive directions. From Fig. 14, we can generally conclude that in the central $2\times 2\times 2\ cm^3$ cube, the magnetic field strength is fairly constant. And the error is determined by divided the difference of magnetic field strength between points zero and 1 cm (or -1 cm) to the total magnetic field strength. The number is within 5% for X axis, 2.5% for Y axis and 2.7% for Z axis.

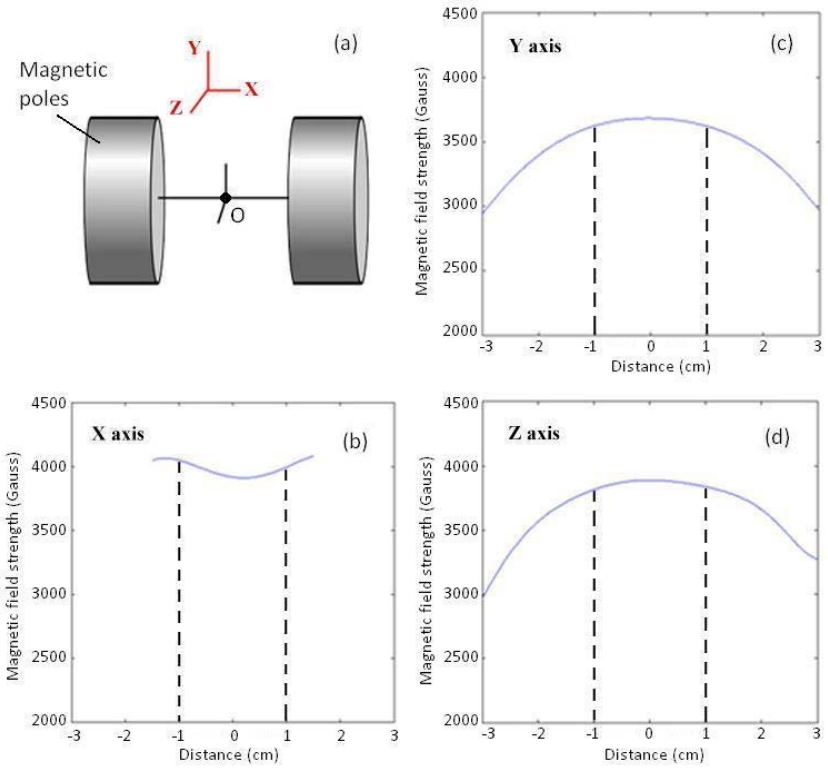

Fig. 14 (a) Sketch of the magnetic poles in three dimensions; (b)the magnetic field strength (Gauss) vs. distance (cm) along axis X; (c) the magnetic field strength vs. distance along axis Y; (d) the magnetic field strength vs. distance along axis Z.

The magnetic probe was inserted between the magnets to test the magnetic field strength via changing the value of potentiometer. The plot is shown in Fig. 15. The potentiometer changes the current supplied to the electromagnets, thus altering the value of the magnetic field strength. According to Fig. 15, the magnetic field strength is approximately linear with respect to the range of the potentiometer. The cryo holder gives a larger magnetic field strength using the same potentiometer setting, because of the smaller distance between the two magnetic poles for the cryo holder. The smaller the distance between the magnets is, the larger the magnetic field. The value of the magnetic field strength in Fig. 15 is comparable to the value obtained from a calibration performed in Sep. 8th, 1995 (potentiometer 900 corresponds to a

magnetic field of 5500 Gauss at room temperature on the holder and to 6500 Gauss in the cryo holder). Therefore, we can conclude that this system has been stable for 16 years.

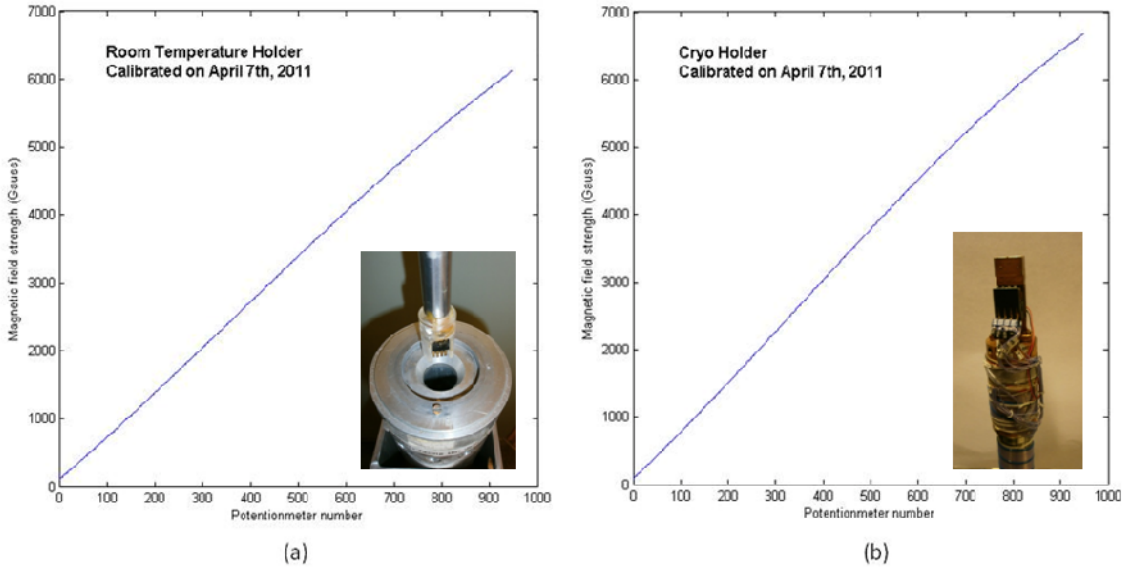

Fig. 15 The magnetic field strength vs. potentiometer setting in (a) Room temperature holder; (b) Cryo holder.

A second Hall effect system is used to verify some of our measurements. This machine is shown in Fig. 16. The sample was inserted into the white plane with four electronic probes contacted with four corners. The back half of the machine supports the magnetic field. The drawback with this system is that it cannot do continuous temperature dependent Hall Effect measurements. Only two temperature points can be obtained from this setup, room temperature and at 77K (liquid nitrogen).

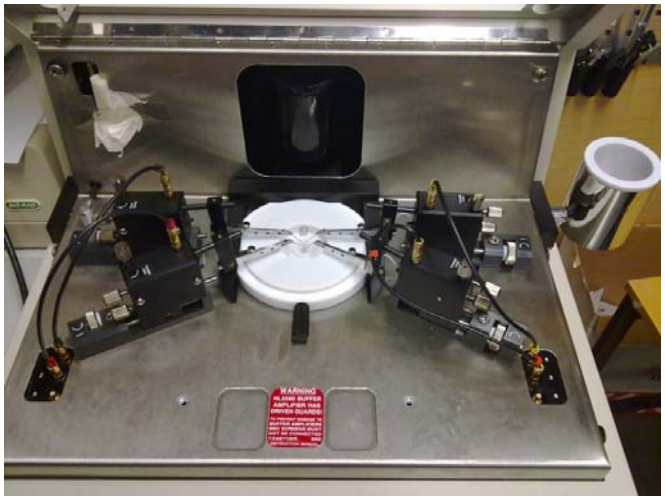

Fig. 16 The Hall Effect machine on 6th floor

6.2 Measurement Procedure

6.2.1 Sample preparation

To measure a new sample, the first step is to check whether the sample is conductive or not on the surface using a multimeter. The sample was cut into $3 \times 3\ mm^2$ pieces using a diamond scriber. For the contact preparation, the sample was placed with the epitaxial layer up. A narrow-tipped soldering iron was used to solder indium on each of the corners. The sample was fixed to the sample holder by a drop of wax. Silver paint was used to connect the soldered indium contacts with the copper strips on the holder. The connections were tested with an Ohmmeter. If all connections gave approximately the same resistance, the sample was ready to be measured. The process is shown in Fig. 17.

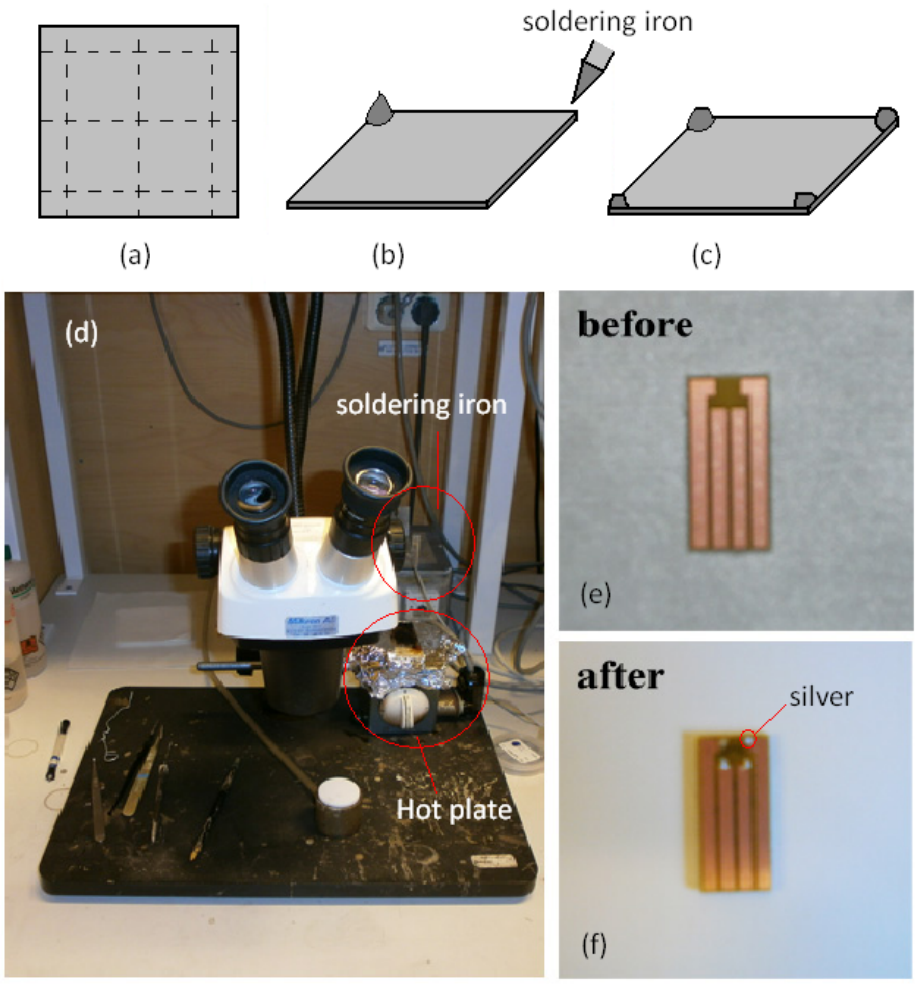

Fig.17 The process of the sample preparation: (a)cutting the sample into $3 \times 3\ mm^2$; (b)making contacts using soldering iron; (c)cutting the sharp tip of the indium contacts; (d) ,(e) and (f) fixing the sample on the holder and using silver paint to connect indium contacts with the copper strips of the holder.

6.2.2 Sample measurement

The sample was mounted into a groove of the chosen holder. The contacts were verified by simply measuring the resistance between the copper leads of the holder. All four should show close to zero resistance. For the cryo holder, there is a protection cap that needs to be screwed on before the measurement. Also a vacuum shield has to be mounted. The turbo pump is used to pump down for at least an hour before starting the cryostat if a low temperature measurement is performed. The software control interface is shown in Fig. 18. Before the measurement, the Hall current needs to be set manually. The magnetic field has to be set manually via the potentiometer. The measurement is started by clicking on "Start Measurement".

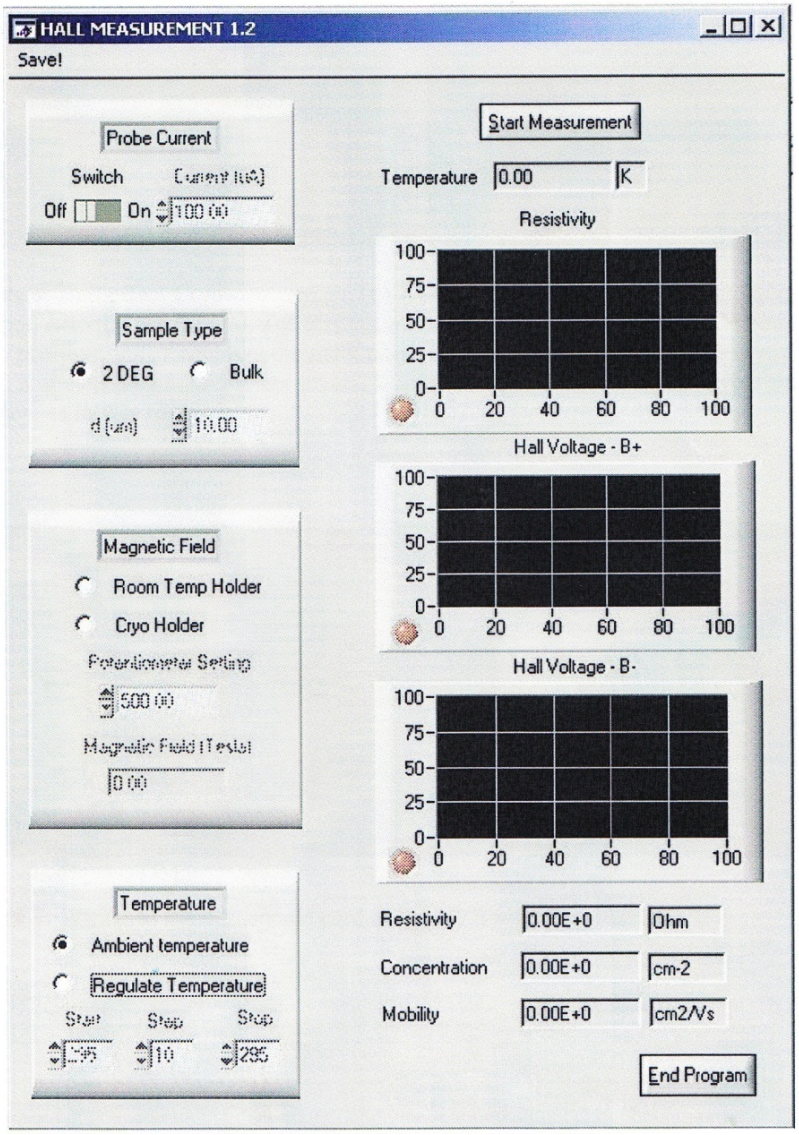

Fig. 18 Computer interface to the Hall Effect program

7. Results and Discussion

Table 5 shows the results of a series of Hall Effect measurements at room temperature. All the samples are GaN grown on GaN templates. GaN template used in our experiments is 3-4 µm insulating GaN layer grown on the sapphire substrate giving the size of circle with diameter of 5 cm. Sample 1550 is insulating. Sample 1547 and 1556 didn't generate a current-voltage (I-V) curve but gives value of the resistivity, mobility and the carrier concentration under the current of 0.1 µA and 0.01 mA respectively. Sample 1603 provides a non-liner I-V curve which gives unreliable values. All other samples are conducting and have a linear I-V contact characteristic for 0.1mA/0.5mA, behaving as ohmic contact in this interval, which is a requirement for reliable Hall effect measurements.

Table 5 Hall Effect measurement results of GaN/GaN in room temperature. Listed is the thickness of the growth layer, the material of growth layer/ template, the Si source temperature (T_{Si}), the resistivity, the mobility and the carrier concentration of the specific sample.

Sample	Thickness (µm)	Material	T_{Si} (°C)	Resistivity (Ω·cm)	Mobility (cm^2/V·s)	Electron carrier Concentration (cm^{-3})
1545	0.7	GaN/GaN	1390	0.0151	48.2	1.19e+19
1546	0.7	GaN/GaN	1350	0.476	29.8	6.16e+17
1547	0.56	GaN/GaN	1300	Bad contacts		
1550	0.7	GaN/GaN	Undoped	Not conducting		
1556	0.14	GaN/GaN	Undoped	Bad contacts		
1557	0.7	GaN/GaN	1390	0.0286	27.7	1.10e+19
1558	0.7	GaN/GaN	1380	0.203	6.78	6.37e+18
1559	0.7	GaN/GaN	1395	0.0175	48.2	1.03e+19
1601	0.294	GaN/GaN	1370	0.169	24.2	1.52e+18
1602	0.456	GaN/GaN	1398	0.00575	89.9	1.21e+19
1603	0.42	GaN/GaN	1330	Non-linear I-V curve		

First, we compare the GaN/GaN samples which are intentional doped by Si source and showing a good conductivity. The carrier concentration as a function of the Si source temperature is shown in Fig. 19. A Si source temperature of 1390 °C resulted in an electron concentration of $1.15 \times 10^{19}\ \mathrm{cm}^{-3}$.

As expected, Fig. 19 shows an exponential relationship between the Si source temperature and the carrier concentration. A change of 10-15 °C of the Si source temperature results approximately in a factor two in the electron concentration. This rate is slightly higher than what has been reported in the literature (a factor two per 15-20 °C). The cause could be a lower sensitivity of the temperature control. The highest carrier concentration was achieved with the Si source at 1398°C which gave a value of $1.21 \times 10^{19}\ cm^{-3}$. This value is very high, when compared to a recent report [68]. Normally, the error of Hall measured carrier concentration has a range from 20% to 50% due to a series of issues such as the imperfect square sample shape, contacts problem and stability of the Hall setup. In Fig. 19, the error bar was performed by 30%. The deviation of the data points is within the expected error limits. This figure is used as a calibration for the GaN:Si layer grown in our MBE system later.

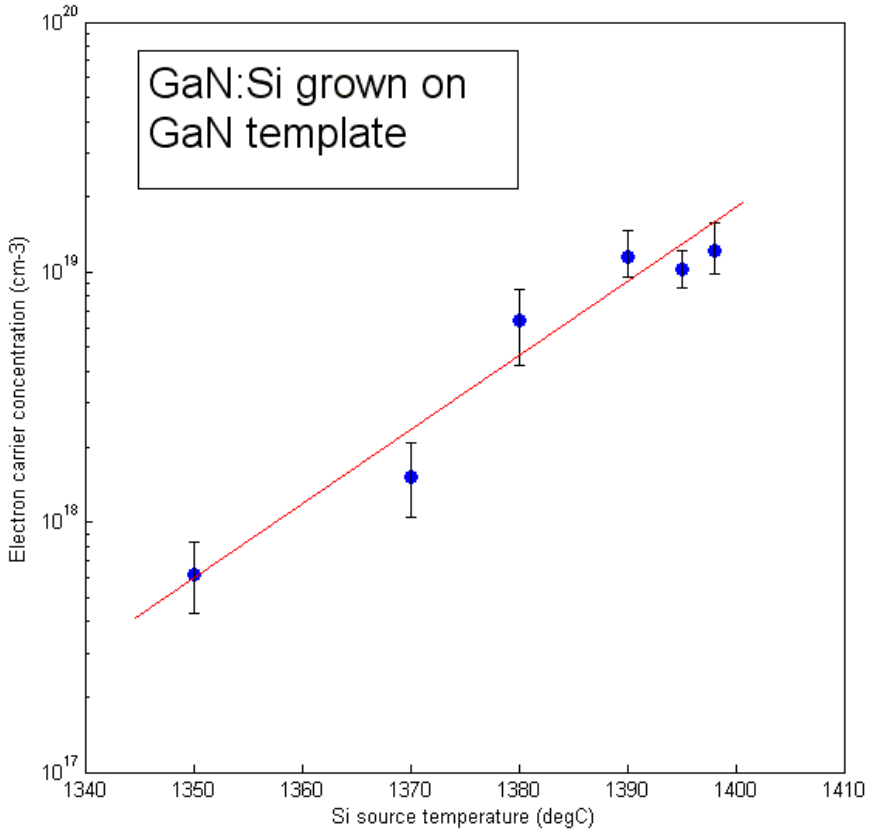

Fig. 19 Electron concentration vs. Si source temperature

We also grew sample 1543, 1601 and 1604 which are GaN grown on different substrates with other parameters staying the same. The results are displayed in Table 6.

Table 6 Hall Effect measurement results of GaN grown on different substrates at room temperature. Listed is the thickness of the growth layer, the material of growth layer/substrate, the Si source temperature (T_{Si}), the resistivity, the mobility and the carrier concentration of the specific sample.

Sample	Thickness (µm)	Material	T_{Si} (°C)	Resistivity (Ω·cm)	Mobility (cm^2/V·s)	Electron carrier Concentration (cm^{-3})
1543	0.5	GaN/Sapphire	1370	0.223	6.67	4.23e+18
1601	0.294	GaN/GaN	1370	0.169	24.2	1.52e+18
1604	0.14	GaN/6H-SiC	1370	2.57e-05	139	1.74e+21

The GaN layer grown on sapphire shows approximately 3 times higher carrier concentration than the sample grown on GaN. This is much higher than expected since the defects related to heteroepitaxy usually results in lower carrier concentrations. We believe that the reason for this high carrier concentration is the growth conditions for GaN/sapphire. Here, an AlN nucleation layer is deposited on the sapphire substrate before the GaN layer is started. The sapphire/AlN/GaN interface can create a 2DEG [69] which will heavily impact the Hall Effect measurements. This is displayed in Fig. 20. The GaN layer grown on sapphire has a defect density that is 10 to 100 times higher than GaN/GaN layers. GaN thin film grown on 6H-SiC shows an ultrahigh carrier concentration of $\sim 10^{21} cm^{-3}$. This is mainly due to the conductive substrate (unintentionally doped). The carrier concentration measured in Hall measurement is the total carrier concentration of both GaN layer and 6H-SiC substrate which is about 300 µm thick. Another reason can be the additive Si doping source from the SiC substrate.

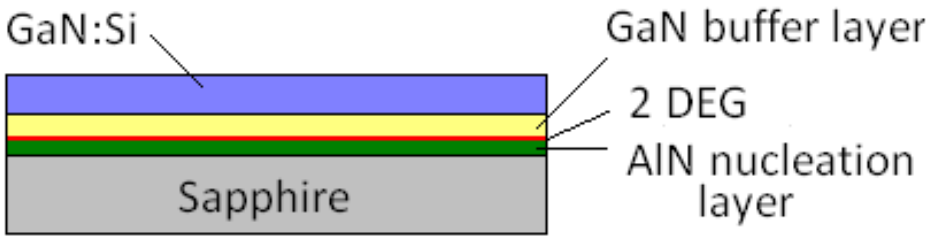

Fig. 20 The diagram of the layer grown in sample 1543 GaN/sapphire.

Table 7 illustrates the results of Hall Effect measurements of AlGaN grown on sapphire template with various compositions of Al and Ga. Sample 1427 is not conductive. The main obstacle refers to the difficulty of Si doping process of the pure AlN materials due to the wide band gap energy (6.2 eV).

Table 7 Hall Effect measurement results of AlGaN with various compositions of Al and Ga. Listed is the thickness of the growth layer, the material of growth layer on sapphire, the Si source temperature (T_{Si}), the resistivity, the mobility and the carrier concentration of the specific sample.

Sample	Thickness (µm)	Material	T_{Si} (°C)	Resistivity (Ω·cm)	Mobility (cm^2/V·s)	Electron carrier Concentration (cm^{-3})
1427	0.5	AlN	1310	Not conducting		
1438	0.5	$Al_{0.1}Ga_{0.9}N$	1350	0.143	33.9	1.28e+18
1439	0.5	$Al_{0.2}Ga_{0.8}N$	1350	0.159	146	2.69e+17
1440	0.5	$Al_{0.3}Ga_{0.7}N$	1350	0.175	64.9	5.49e+17

From table 7, we see that the highest carrier concentration was achieved by $Al_{0.1}Ga_{0.9}N$. As have been observed previously by others [70], the free carrier concentration in Si-doped AlGaN alloys decreases as the Al content is increased, because of the difficulties in AlGaN. In our work, an electron concentration as high as $1.28 \times 10^{18} cm^{-3}$ and resistivity as low as 0.143 Ω·cm have been determined by room temperature Hall measurement for sample 1438. The resistivity is a significant higher than the MOCVD grown $Al_{0.1}Ga_{0.9}N$ films reported earlier having a resistivity of $\sim 10^{-3} \Omega \cdot cm$. Also the carrier concentration is lower compared to $8.8 \times 10^{18} cm^{-3}$ found in the literature [71]. Sample 1440 is comparable to the literature [72]. Here they grew a 1.8 µm Si doped $Al_{0.3}Ga_{0.7}N$ layer which showed a carrier concentration of $3 \times 10^{18} cm^{-3}$ and an excellent mobility of 80 cm^2/V·s. It was expected that sample 1439 have a carrier concentration value between samples 1438 and 1440. Instead it had the lowest carrier concentration. The reason could be the Si source which has a performance that fluctuates over time.

Sample MBE-II-175 is an n-type GaAs layer, used as a reference sample in this diploma work for checking the stability of the Hall setup. It gives a resistivity of 0.878 Ω·cm, a mobility of 7707.8 cm^2/Vs and a carrier concentration of $9.22 \times 10^{14}\ cm^{-3}$ at room temperature. We performed temperature dependent Hall Effect measurements on this sample. The results are displayed in Fig. 21.

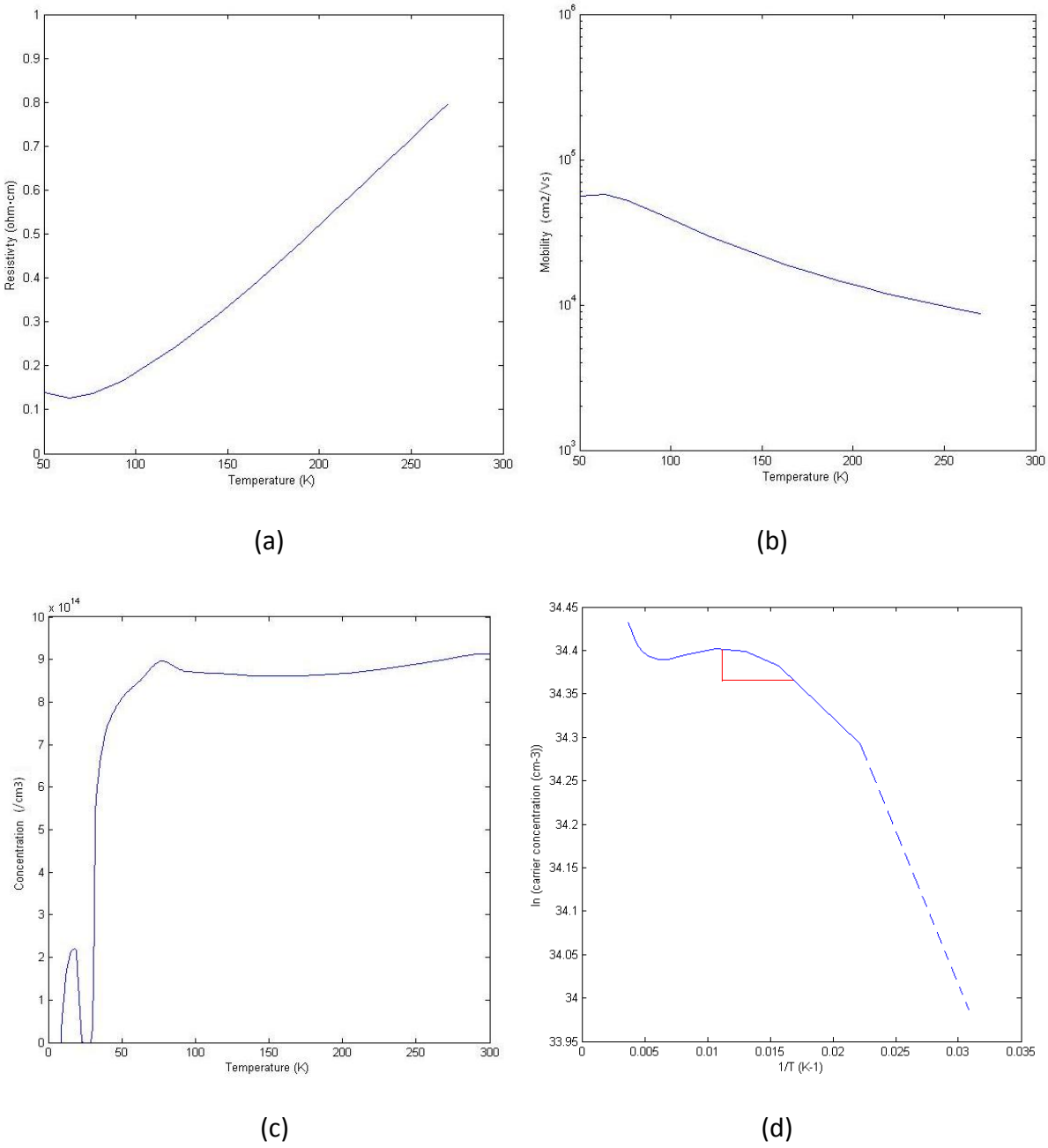

Fig. 21 Temperature dependent Hall measurements on a GaAs layer (a) resistivity vs. temperature; (b) mobility vs. temperature; (c) carrier concentration vs. temperature and; (d) Arrhenius plot for calculation of the donor activation energy.

From Fig. 21, we can conclude that only mobility declines with increased temperature. The resistivity and carrier concentration increase with temperature. In Fig. 21 (c), a dramatic decrease is found when the temperature around 60 K. In room temperature (300 K), the thermodynamic energy kT is about 25.8 meV. For the GaAs doped with Si, the activation energy is 5.8 meV (Table 2) corresponding to the temperature of 67 K. Thus when the temperature goes down to 67 K, the thermodynamic energy is not large enough to excite the Si donors to the conduction band of GaAs and the carrier concentration falls down to close to zero. And 67 K is the so called freeze out temperature. In practice, the carrier concentration cannot fall to zero immediately. But we still observe a significant decrease from 60 K and finally to zero at 30 K. Other large fluctuations occur in the curve and are probably due to the instability of the Hall setup.

An Arrhenius plot is used as a common way to present data. According to Arrhenius equation:

$$k = Ae^{-E_a/k_BT}$$

Where k is the rate constant, k_B is the Boltzmann constant, T is the absolute temperature and E_a is the activation energy. We plot the logarithmic of the carrier concentration as a function of the inverse of the absolute temperature. The Arrhenius plot based on our sample is displayed in Fig. 21(d). By taking the logarithm of the Arrhenius equation, the slope of the Arrhenius plot can be expressed as $-\frac{E_a}{k_B}$.

In Fig. 21 (d), the slope of Arrhenius plot is about -37.3. The activation energy of GaAs is calculated as below

$$E_a = 37.3 \times k_B = 3.23\, meV.$$

When comparing this value to 5.8 meV, it turns out a difference but still within our expected. The reason could be various mainly due to the uncertain issues of the Hall setup.

We are planning to do the similar temperature dependent Hall measurement on the previous GaN:Si/GaN samples and also calculate the activation energy of GaN material. Unfortunately, the Hall setup did not work well after finishing this GaAs:Si experiments.

8. Summary and Future Work

This thesis work has been done in the Photonics and Microwave Electronics Laboratories in the Department of Microtechnology and Nanoscience (MC2) at Chalmers University of Technology during the first half of year 2011. In this study, electrical characterizations of GaN and AlGaN thin films doped with Si source were investigated by Hall effect measurements.

GaN:Si grown by MBE system shows an increasing carrier concentration when the Si source cell temperature is increased. The highest carrier concentration of GaN:Si was obtained at Tsi= 1398 °C, yielding a value of $1.21 \times 10^{19}\ cm^{-3}$. The highest measured mobility is 89.9 cm^2/V·s, which is within the demands of device applications. GaN:Si grown on different templates showed various conductive properties mainly due to the defects caused by the lattice-mismatch. A 2DEG behavior was observed during the measurement of the GaN/sapphire sample. It was suggested that the AlN nucleation layer deposited on the sapphire substrate generates an AlN/GaN heterostructure.

AlGaN:Si alloys with different Al content were also studied. The carrier concentration decreases as the Al content is increased. The difficulties in doping AlGaN alloys with higher Al content is well known and was confirmed by this experiments. The measurement values obtained from our work group were much reasonable compared to the literature.

Due to time constraints and a catastrophic failure of the Hall (and the capacitance-voltage (CV) setup), temperature dependent Hall effect measurements were only performed on the reference GaAs sample.

GaN grown on SiC templates is another suggestion for future work. Insulating SiC templates should be used to remove the effects from the substrate.

With decreasing Si source temperature, the carrier concentration of GaN/GaN decreases slightly faster than what has been reported in the literature. The cause for this effect is as the present unknown and needs more investigation. CV measurement is a valuable tool that can be used to learn more details about the electrical properties of GaN:Si and AlGaN:Si.

Reference

[1] G. Busch, “Early history of the physics and chemistry of semiconductors – from doubts to fact in a hundred years”, *Eur. J. Phys.*, vol. 10, no. 4, pp. 254–263, 1989.

[2] F. Laeri, F. Schüth, U. Simon, and M. Wark, *Host-Guest-Systems Based on Nanoporous Crystals*. Weinheim: Wiley, 2003, pp. 435–436.

[3] T. K. Sarkar, R. Mailloux, A. A. Oliner, M. Salazar-Palma, and D. L. Sengupta, *The History of Wireless*. Hoboken: Wiley, 2006.

[4] W. Mönch, *Semiconductor Surfaces and Interfaces*. Berlin-Heidelberg: Springer, 2001.

[5] Z. A. Smith and K. D. Taylor, *Renewable and Alternative Energy Sources: A Reference Handbook*. Santa Barbara: ABC-CLIO Inc., 2008, p. 157.

[6] J. Perlin, *From Space to Earth: The Story of Solar Electricity*. Cambridge: Harvard University Press, 2002, p. 17.

[7] L. Hoddeson, E. Braun, J. Teichmann, and S. Weart, *Out of the Crystal Maze: Chapters in the History of Solid State Physics.* New York: Oxford University Press, 1992.

[8] F. Fichter, Uber Aluminiumnitrid, Z. Anorg. Chem. 54, 322, 1907.

[9] J.V. Lirmann and H.S. Schadanov, Acta Physicochim. URSS 6, 306, 1937.

[10] H.P. Maruska and J.J. Tietjen, *Appl. Phys. Lett*, 15, 327, 1969.

[11] J.I. Pankove, E.A. Miller, and J.E. Berkeyheiser, RCA Rev. 32, 383, 1971.

[12] H.M. Manasevit, F.M. Erdmann, and W.I. Simpson, J. *Electorchem. Soc*, 118, 1864, 1971.

[13] R. Dingle, K.L. Shaklee, R.F. Leheny, and R.B. Zetterstrom, *Appl. Phys. Lett*, 19, 5, 1971.

[14] S. Yoshida, S. Misawa, and S. Gonda, Appl. Phys. Lett. 42, 427, 1983.

[15] H. Amano, N. Sawaki, I. Akasaki, and Y. Toyoda, Appl. Phys. Lett. 48, 353, 1986.

[16] S. Nakamura, Japn. J. Appl. Phys. Part 2, 30, L1705, 1991.

[17] H.Amano, M. Kito, K. Hiramatsu, and I. Akasaki, Jap. J. *Appl. Phys*, 28, L2112, 1989.

[18] S. Nakamura, T. Mukai, M. Senoh, and N.Iwasa, Jpn. J. *Appl. Phys*, 31, L139, 1992.

[19] S. Nakamura, T. Mukai, M. Senoh, S. Nagahama, and N. Iwasa, J. *Appl. Phys*, 74, 3911, 1993.

[20] M.A. Khan, S. Krishnankutty, R.A. Skogman, J.N. Kuznia, and D.T. Olson, *Appl. Phys. Lett*, 65, 520, 1994.

[21] S.T. Kim, H. Amano, ans I. Akasaki*, Appl. Phys. Lett*. 67, 267, 1995.

[22] H. Amano, *Appl. Phys. Lett*, 64, 1377, 1994.

[23] A.S. Zubrilov*, Appl. Phys. Lett*, 67, 533, 1995.

[24] S. Nakamura, *Jpn. J. Appl. Phy,.* 35, L74, 1996.

[25] I. Akasaki, Electon. Lett. 32, 1105, 1996.

[26] S. Nakamura, *Appl. Phys. Lett*, 72, 2014, 1998.

[27] M.A. Khan, J.N. Kuznia, A.R. Bhatarai, and D.T. Olsen, *Appl. Phys. Lett*, 62, 1786, 1993.

[28] J.I. Pankove, S.S Chang, H.C. Lee, R. Molnar, T.D. Moustakas, and B. van Zeghbroeck, Tech. Dig. Int. Electron Devices Meet. 94, 389, 1994.

[29] R. Gaska, J.W. Yang, A. Osinsky, Q. Chen, M.A. Khan, A.O. Orlov, G.L. Snider, and M.S, Shur, Appl. Phys. Lett. 72, 707, 1998.

[30] M.S. Shur, http://nina.ecse.rpi.edu/shur/nitride.

[31] S. Strite and H. Morkoc. Journal of Vacuum Science & Technology B, microelectronics Processing and Phenomena, 10(4): 1237-66, 1992.

[32] S. Strite, G.B. Gao, M. Burns (1994), "Large-band-gap SiC, III-V nitride, and II-VI ZnSe-based semiconductor device technologies", *Journal of* Applied Physics, 1994.

[33] http://powerelectronics.com/passive_components_packaging_interconnects/resistors/sic-gan-vie-slice-electric-vehicle-pie-20091101/

[34] R. He, Y. Zhang, S. Lee and P. Yang, "Single-crystal gallium nitride nanotubes", *Nature* 422 (6932): 599–602, 2003.

[35] S.M. Sze, “Physics of Semiconductor Devices (2nd Edition)”, *Wiley-Interscience*, p. 9-11, September, 1981.

[36] http://www-opto.e-technik.uni-ulm.de/lehre/cs/

[37] H. Masui, Nonpolar and semipolar III-nitrides light-emitting diodes: achievements and challenges, *IEEE Transactions on electron devices*, Vol.57, No.1, Jan 2010.

[38] Donald A. Neamen, *Semiconductor Physics and Devices: Basic Principles (2nd Edition),* January 1, 1997.

[39] S.M. Sze, "Physics of Semiconductor Devices (2nd Edition)", *Wiley-Interscience*, p. 304-306, September, 1981.

[40] Thorvald Andersson, "Semiconductors and Heterostructures", textbook of Semiconductor Material Physics, p.115-116, 2010.

[41] D. R. Lide, CRC Handbook of Chemistry and Physics, 77th ed. Boca Raton, FL: CRC Press, pp. 12–122, 1996.

[42] June O Song, Jun-Seok Ha, and Tae-Yeon Seong, "Ohmic contact Technology for GaN-Based Light-Emitting Diodes: Role of P-Type Contact", *IEEE Transations on Electron Devices*, Vol.57, No.1, Jan. 2010.

[43] W. Götz, N. M. Johnson, J. Walker, D. P. Bour, and R. A. Street, "Activation of acceptors in Mg-doped GaN grown by metalorganic chemical vapor deposition," *Appl. Phys. Lett.*, vol. 68, no. 5, pp. 667–669, Jan. 1996.

[44] H. Ishikawa, S. Kobayashi, Y. Koide, S. Yamasaki, S. Nagai, J. Umezaki, M. Koike, and M. Murakami, "Effects of surface treatments and metal work functions on electrical properties at p-GaN/metal interfaces," *J. Appl. Phys.*, vol. 81, no. 3, pp. 1315–1322, Feb. 1997.

[45] Y. Koide, T. Maeda, T. Kawakami, S. Fujita, T. Uemura, N. Shibata, and M. Murakami, "Effects of annealing in an oxygen ambient on electrical properties of ohmic contacts to p-type GaN," *J. Electron. Mater.*, vol. 28, no. 3, pp. 341–346, Dec. 1999.

[46] I.V. Abarenkov and V. Heine, "The model potential for positive ions", *Philosophical Magazine* 12, 529, 1965.

[47] E.F. Schubert, "Physical Foundations of Solid-State Devices", *Rensselaer Polytechnic Institute*, P. 1-18, Chapter 15, 2009.

[48] Thorvald Andersson, "Semiconductors and Heterostructures", textbook of Semiconductor Material Physics, p.50, 2010.

[49] J. Singh, "Physics of Semiconductors and their Heterostructures", *McGraw-Hill*, New York, 1993.

[50] E.H. Hall, *On a New Action of the Magnet on Electrical Current*, Amer. J. Math.2, 287-292, 1879.

[51] A.C. Beer, "The Hall Effect and Related Phenomena", *Solid-State Electronics*, Vol.9, 339-351, 1966.

[52] B.I. Bleaney, "Electricity and Magnetism (2nd Edition*)", Oxford University Press, Ely House*, London, Chapter 3, 61, 1965.

[53] S.O. Kasap, Hall Effect in Semiconductors, *e-Booklet*, 2001.

[54] M.M. Cumming, Hall Effect Measurements on GaAs and InSb Grown by Molecular Beam Epitaxy, *Department of Physics*, Chalmers University of Technology, 1991.

[55] D.C. Look, *Electrical Characterization of GaAs Materials and Devices*, 13-14(1989).

[56] D.C. Look, *Electrical Characterization of GaAs Materials and Devices*, 9-12(1989).

[57] http://course.tju.edu.cn/physics/syjx/jxnr/cha3/s19.html

[58] R.A. Stradling and P.C. Klipstein, "Growth and Characterization of Semiconductors", *IOP Publishing Ltd,* 1990.

[59] R. Fernando, *Basics of Molecular Beam Epitaxy (MBE)*, Annual Report 2002, Optoelectronics Department, University of Ulm.

[60] http://gorgia.no-ip.com/phd/html/thesis/phd_html/node4.html

[61] Thorvald Andersson, "Semiconductors and Heterostructures", textbook of Semiconductor Material Physics, p.163-167, 2010.

[62] http://www.tmi.vu.lt/legacy/pfk/funkc_dariniai/technology.htm

[63] O.Oda, T.Inque and etc., *Physica Status Solidi A*, 180(1):51-8, 2000.

[64] L. Liu, J. H. Edgar, Substrates for gallium nitride epitaxy, Materials Science and Engineering: R: Reports, Volume 37, Issue 3, P. 61-127, 30 April 2002.

[65] N.Grandjean, J.Massies and R.A. Talalaev, *Applied Physics Letters*, 74(13):1854-6, 1999.

[66] Z. Y. Fan and N. Newman, *Materials Science & Engineering B: Solid-State Materials for Advanced Technology*, 87(3):244-248, 2001.

[67] B.Heying, R.Averbeck, L.F. Chen and J.S. Spect*, Journal of Applied Physics*, 88(4):1855-60, 2000.

[68] S.C. Jain, M.Willander, J. Narayan, and R.V.Overstraeten, *Applied Physics*, 87, 965, 2000.

[69] F. Medjdoub, M. Zegaoui, D. Ducatteau, N. Rolland, and P.A. Rolland, "High-Performance Low-Leakage-Current AlN/GaN HEMTs Grown on Silicon Substrate", *IEEE Electron Device Letters*, Vol. 32, No.7, Jul. 2011.

[70] C.J. Eiting, P.A. Grudowshi, and R.D. Dupuis, "P- and N-Type Doping of GaN and AlGaN Epitaxial Layers Grown by Metal Organic Chemical Vapor Deposition", *Journal of Electronic Materials*, Vol. 27, No.4, 1998.

[71] S, Jinqiao, R. Anthony, T. James, M. Seiji, D. Rafael and S. Zlatko, "Progress on n-type doping of AlGaN alloys on AlN single crystal substrates for UV optoelectronic applications", Phys, Status Solidi C 8, No. 7-8, 2031-2033, Dol 10.1002, pssc. 201000964, 2011.

[72] Y.A. Xi, K.X. Chen, and etc., "Comparative study of n-type AlGaN grown on sapphire by using a superlattice layer and a low-temperature AlN interlayer", *Journal of Crystal Growth*, 299, 59-62, 2007.